BNL-219848-2020-TECH
C-A/AP/633

Imperfection resonance crossing in the AGS Booster

K. Hock

September 2020

Collider Accelerator Department
Brookhaven National Laboratory

U.S. Department of Energy
USDOE Office of Science (SC), Nuclear Physics (NP) (SC-26)

DISCLAIMER

Imperfection resonance crossing in the AGS Booster

K. Hock, F. Méot, H. Huang, N. Tsoupas
BNL C-AD, Upton, NY 11973

September 14, 2020

Abstract

Polarized helions are part of the spin physics program for the EIC, allowing collisions of polarized neutrons with polarized electrons [1, 2]. Helion imperfection resonances are 2.4 times closer than protons. Helions cross two intrinsic resonances ($|G\gamma| = 12 - \nu_y$ and $|G\gamma| = 6 + \nu_y$) and six imperfection resonances ($|G\gamma| = 5,\ 6,\ 7,\ 8,\ 9$, and 10) in the Booster as they are accelerated to extraction at $|G\gamma| = 10.5$. In this same range of γ, protons cross two imperfection resonances ($|G\gamma|$=3, and 4) and are extracted from the Booster prior to crossing the $|G\gamma| = 0 + \nu_y$. Preliminary benchmarking simulations are performed using protons crossing the $|G\gamma| = 3$ and 4 imperfection resonances, results of which are compared to experimental data. The settings used for protons are extrapolated to the helion case to show there is sufficient corrector strength to preserve polarization at each imperfection resonance up to extraction.

1 Imperfection Resonances

Imperfection resonances result from a non-zero closed orbit that causes the particles to sample the horizontal field in quadrupoles. These resonances occur when the spin tune is equal to an integer,

$$\nu_s = |G\gamma| = k \tag{1}$$

where k is an integer, G is the anomalous magnetic moment ($G_{helions} = -4.18415$ and $G_{protons} = 1.79285$), γ is the Lorentz factor, and ν_s is the spin tune. Polarized helions are injected into the Booster at $|G\gamma| = 4.19$ from the EBIS and are ideally extracted at $|G\gamma| = 10.5$. In this range, polarized helions will encounter six imperfection resonances ($|G\gamma| = 5,\ 6,\ 7,\ 8,\ 9,\ 10$) as they are accelerated to $|G\gamma| = 10.5$. Helion imperfection resonances are separated by

$$\frac{M_o/u}{G} = 223.73 \text{ MeV/u}. \tag{2}$$

The imperfection resonance strength is [3],

$$\epsilon_k = \frac{1+G\gamma}{2\pi} \oint \frac{\frac{\partial B_x}{\partial y}}{B\rho} y_{co} e^{iK\theta} ds \tag{3}$$

where $\partial B_x/\partial y$ is the quadrupole gradient field, $B\rho$ is the rigidity, K is the resonance condition (which in this case corresponds to K=k), and θ is the orbital bending angle. It is worthwhile to note that the vertical closed orbit error is,

$$y_{co} = \sqrt{\beta_y(s)} \sum_{k=-\infty}^{\infty} \frac{\nu_y^2 f_k}{\nu_y^2 - k^2} e^{ik\phi_y(s)}. \tag{4}$$

where β_y is the vertical betatron function through the ring, ν_y is the vertical betatron tune, ϕ_y is the vertical betatron phase, and f_k is the stopband integral [4]. For correcting the $|G\gamma| = k$ resonance, the h=k harmonic of the corrector dipoles is used. The harmonic correction method is described in detail in Sec. 2.

The resonance strengths are calculated using three methods: Eq. 3, Froissart-Stora formula, and the Static method. The Froissart-Stora formula is defined as,

$$\frac{P_f}{P_i} = 2\exp\left(\frac{-\pi|\epsilon_k|^2}{2\alpha}\right) - 1 \tag{5}$$

where α is the resonance crossing speed, and P_i and P_f are the asymptotic values of the polarization before and after crossing the resonance. The resonance crossing speed is defined as,

$$\alpha = \frac{dG\gamma}{d\theta}. \tag{6}$$

and for protons $\alpha_{protons} = 5.105 \times 10^{-6}$, where for helions there is a fast, $\alpha_{helions,fast} = 7.961 \times 10^{-6}$, and slow crossing speed, $\alpha_{helions,slow} = 2.654 \times 10^{-6}$. The Froissart-Stora allows predicting the final polarization at a given resonance, k, and harmonic, h=k, as a function of corrector current using [3],

$$\frac{P_f}{P_i} = 2\exp\left[-\frac{(I_{k,\sin} - I_{k,o\sin})^2}{2\sigma_{k,\sin}^2}\right]\exp\left[-\frac{(I_{k,\cos} - I_{k,o\cos})^2}{2\sigma_{k,\cos}^2}\right] - 1 \tag{7}$$

where $I_{k,\sin}$ and $I_{k,\cos}$ are the corrector dipole current for the two corrector families, $I_{k,o\sin}$ and $I_{k,o\cos}$ are the optimal corrector currents for the two corrector families, and $\sigma_{k,\sin}$ and $\sigma_{k,\cos}$ are the RMS widths for the two families. Note this equation is Gaussian. The currents $I_{\sin}$ and $I_{\cos}$ for harmonic h will be referred to as sinhv and coshv.

The formula for the Static method is defined as,

$$\bar{S_y}^2 = \frac{1}{1 + |\epsilon_k|^2/\Delta^2} \tag{8}$$

where $\Delta = |G\gamma| - K$ is the distance between $|G\gamma|$ and resonance K. The calculated resonance strengths are shown in Tab. 1, and the relevant tracking results shown in Sec. A.2.1 and Sec. A.2.2.

Table 1: Summary of imperfection resonance strengths for protons and helions with quadrupole alignment based on Fig. 1a.

Species	k	$B\rho$ $[T \cdot m]$	ϵ_k		
			Froissart-Stora	Static	Eq. 3
Protons	3	4.198	0.000737	0.000714	0.000644
	4	6.240	0.002238	0.002367	0.002396
Helions	5	3.064		0.004605	0.004492
	6	4.814	0.000684	0.000701	0.000716
	7	6.282	0.001283	0.001299	0.001158
	8	7.633	0.003444	0.003582	0.003834
	9	8.920	0.000223	0.000226	0.000239
	10	10.167		0.006252	0.006646

2 Harmonic Correction

To preserve polarization through a resonance at $|G\gamma| = k$, the corresponding harmonic, h=k, must either be corrected so no polarization is lost, or enhanced to induce a full spin-flip. The Booster has 24 vertical orbit correctors, placed adjacent to vertically focusing quadrupoles, and are used for creating and correcting orbit harmonics. These corrector magnets are 10 cm long with an excitation of 0.975 $G \cdot m/A$, where the supplies have a maximum current of 25 A [5].

These correctors are powered according to [4]

$$B_{j,h} = a_h \sin(h\theta_j) + b_h \cos(h\theta_j) \tag{9}$$

where j is corrector number, θ_j is the location in the ring, a_h and b_h are the amplitudes for harmonic h.

The primary source of these orbit errors that require correction are from alignment errors of the quadrupoles, causing particles to sample the depolarizing horizontal fields. These alignment errors, Fig. 1a, were placed into a zgoubi input file to allow comparison of simulation data with experimental data.

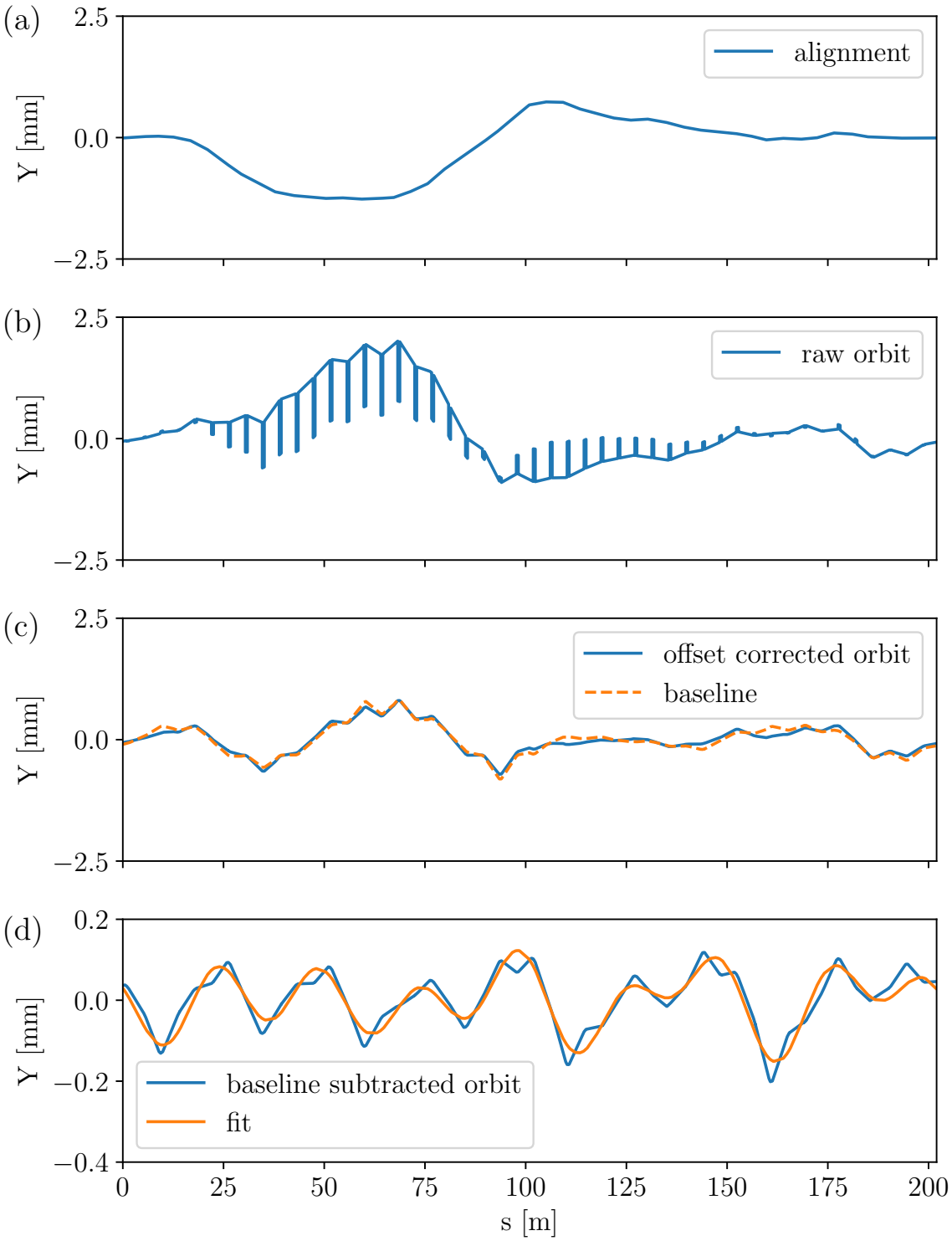

Figure 1: a) Vertical quadrupole misalignments in the Booster are scaled to 65% to match h=4 data, Fig. 5; b) orbit output from zgoubi where discontinuities result from the use of CHANGREF through quadrupoles; c) Orbit after incorporating misalignments; d) Baseline subtracted orbit for helions crossing the $|G\gamma| = 8$ resonance after the h=4, 5 harmonics have been corrected with the addition of h=8. This example has a corrector current with respect to h=8 of cos8v=5 A, sin8v=13 A. The components of the fit results are: [sin4, cos4, sin5, cos5, sin8, cos8]=[-0.0512 A, 0.0043 A, 0.00042 A, -0.0036 A, -0.0031 A, 0.0061 A].

For helions, the h=4 orbit is corrected at $|G\gamma|$=5 and the correction from the h=5 harmonic scan is scaled to all higher order resonances by the ratio of rigidity. That is I(h=5,$|G\gamma|$=k)=I($|G\gamma|$=5) $B\rho(|G\gamma| = k)/B\rho(|G\gamma| = 5)$. This allows all helion imperfection resonances to be studied with the same orbit seen in Fig. 1c. The resulting orbit after introducing h=8 into the corrector dipoles and correcting the h=4, 5 orbits is shown in Fig. 1d. These currents are [sin4v, cos4v, sin5v, cos5v]=[2.797, 0.669, 0.520, 4.296] and scaled up appropriately to the resonance being simulated.

The total current on corrector j is

$$I_j = \sum_h I_{h,\sin} \sin(h\theta_j) + I_{h,\cos} \cos(h\theta_j) \tag{10}$$

where $I_{h,\sin}$ and $I_{h,\cos}$ are the equivalent of sinhv and coshv. This is used to determine the total current on each of the correctors, where the maximum current of all correctors is

$$I_{max} = \max[|I_j|]. \tag{11}$$

This is an important parameter so as to avoid exceeding the maximum current allowed by the corrector supplies. A study of the magnetic property of the dipoles performed in 1994 powered the magnets to 50 A but reported heating issues if powered for long periods of time [5].

These harmonic correctors are controlled via the *boosterOrbitControl* application shown in Fig. 2. The amplitude of the desired harmonics can be manipulated at specific times in the cycle to reach the desired correction. For the harmonic scans, the amplitude is adjusted at the time in the cycle corresponding to the resonance being crossed. Each corrector has a gain which is the scaling factor, relative to the desired amplitude, dependant on its phase. This gain is the equivalent of the $\sin(h\theta_j)$ or the $\cos(h\theta_j)$ depending on which component is being corrected.

3 Harmonic Scans

3.1 Proton Harmonic Scans

At the onset of a polarized proton run for RHIC, a harmonic scan is performed in Booster to ensure that polarization transmission is optimal. These scans involve collection of data at various corrector currents, but with the corrector current in the orthogonal family being fixed. The dataset being used was taken on January 12, 2017 with the scans performed as: sin3v currents scanned between -4.8 and 5.2 with cos3v=-6.5; cos3v scanned between -13.0 and 9.0 with sin3v=0.2; sin4v scanned between -10.0 and 10.0 with sin3v=-6.5, cos3v=0.2, and cos4v=2.0; cos4v scanned between -20 and 10 with sin3v=-6.5, cos3v=0.2, sin4v=1.6. These scans are recreated using zgoubi in an effort to improve the model so it

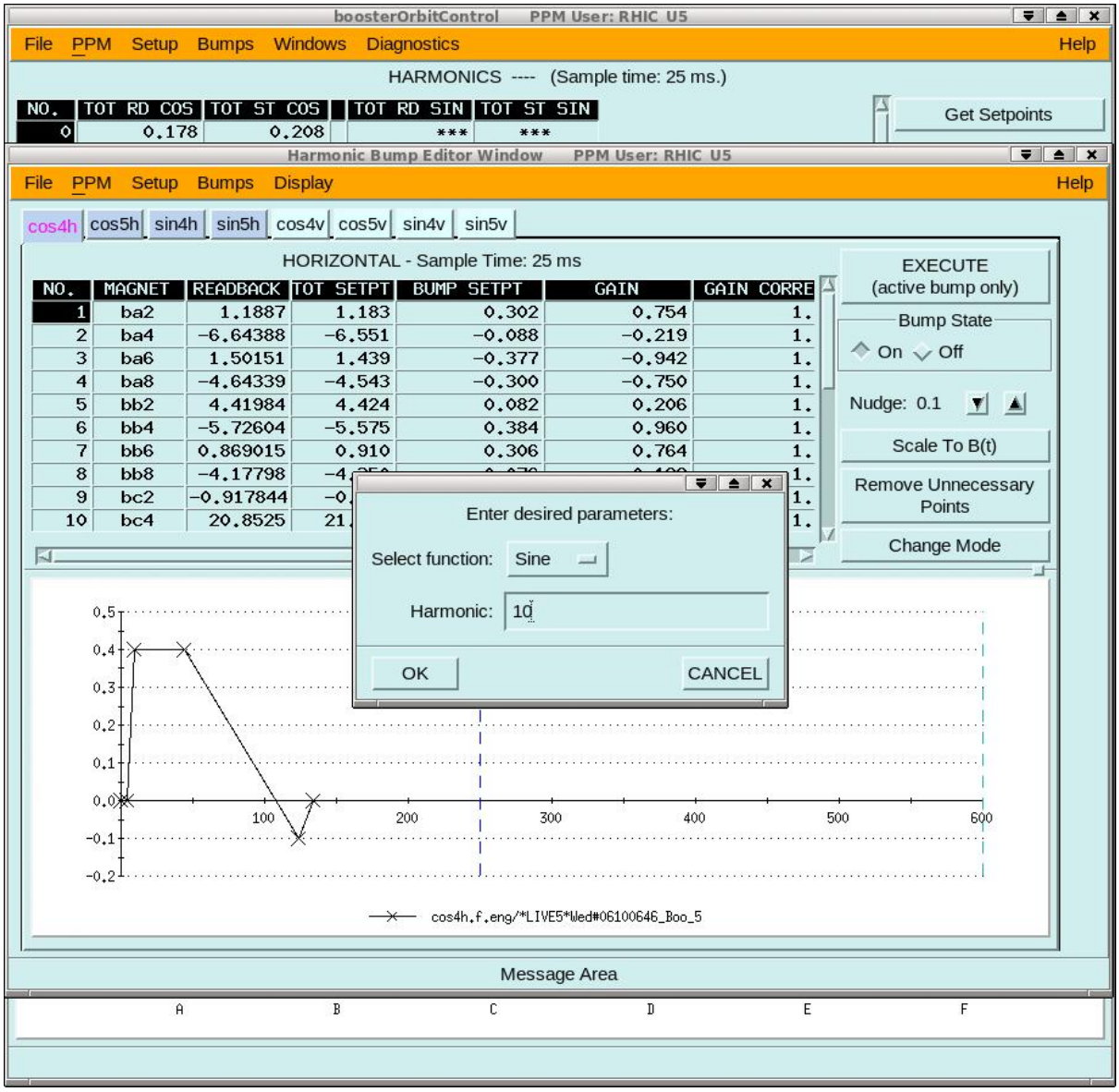

Figure 2: Image of the *boosterOrbitControl* application for the Au user during RHIC run 20. The active harmonics are h=4 and h=5 for the horizontal and vertical planes. The window in the center of the image shows that any desired harmonic may be entered and manipulated.

gives accurate results and determine the corrector current required for each of the helion resonances.

3.1.1 Single and Dual Dipole Error

Since a single dipole error excites all orbit harmonics, one can simulate harmonic scans using individual quadrupole misalignments. Best results are obtained with two misaligned quadrupoles that are $\pi/2$ away from each other with respect to the harmonic of interest.

The closed orbit error resulting from a single dipole error is,

$$y_{co}(s) = \frac{\sqrt{\beta_y(s)\beta_y(s_o)}}{2\sin(\pi\nu_y)}\cos(\pi\nu_y - |\psi(s) - \psi(s_o)|)\theta(s_o) \tag{12}$$

where s_o is the location of the error, s is the location around the ring, $\theta(s_o)$ is the kick angle, and

$$\psi_s = \int_0^s \frac{1}{\beta_y(s)} ds. \tag{13}$$

For h=4, a harmonic period is 12 cells. An example harmonic scan is shown in Fig. 3 which has D7 misaligned vertically by -1.1 mm. For two misaligned quadrupoles, A4 is also misalgined by -6.3 mm. Note these are $\pi/2$ away from each other with regard to the harmonic phase. It was found that any two quadrupoles with the appropriate harmonic phase and separated by $\pi/2$ could match harmonic scan data by varying their two amplitudes. This creates an interference modification to Eq. 14 that is

$$y_{co}(s) = \frac{\sqrt{\beta_y(s)\beta_y(s_o)}}{2\sin(\pi\nu_y)}\cos(\pi\nu_y - |\psi(s) - \psi(s_o)| + \phi)\theta(s_o) \tag{14}$$

that introduces a phase offset, ϕ, for the closed orbit. This is from the identity that

$$A\cos(\theta) + B\sin(\theta) = C\cos(\theta + \phi) \tag{15}$$

where the addition of cos and sin with amplitudes A and B can be represented with a cos function with amplitude C with a phase offset ϕ.

Extending this application of varying individual quadrupoles is problematic due to the quadrupoles needing to be in phase with each of the harmonics and also their varied amplitude. This increases the number of misaligned quadrupoles needed to be able to match the n harmonic scans.

3.1.2 Quadrupole Misalignment

The quadrupoles were misaligned according to the data shown in Fig. 1a [6]. The pyzgoubi input file reads the spreadsheet that contains the alignment data and uses the zgoubi keyword CHANGREF, which changes the position of the particles relative to the quadrupoles. The effect of CHANGREF on the orbit is seen in Fig. 1b. Results from these simulation and comparison to experimental data is shown in Fig. 4 and Fig. 5. The harmonic scan data is fit with a Gaussian defined as

$$S_y(I) = B\exp\Big[-\frac{(I-\mu_f)^2}{2\sigma_f^2}\Big] \tag{16}$$

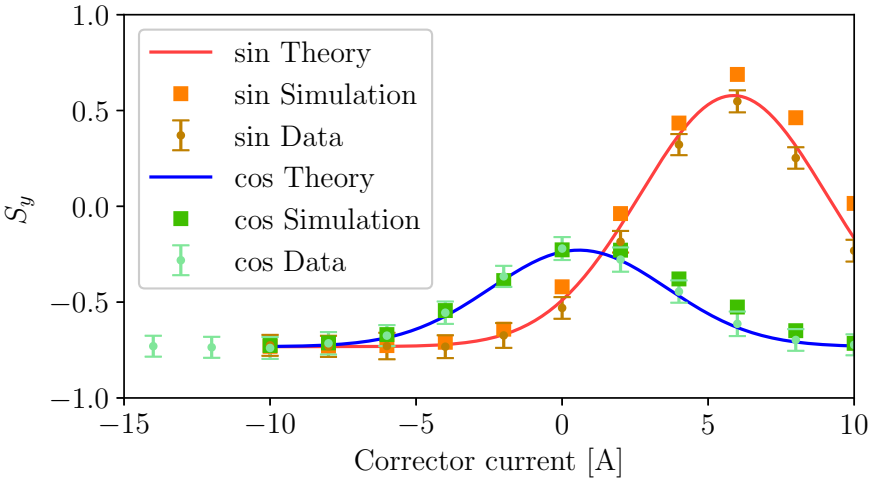

Figure 3: Simulation of protons crossing $|G\gamma| = 4$ with a single misaligned quadrupole, D7=-1.1 mm.

with f is the sine or the cosine corrector family, μ_f is the location of the peak corresponding to the optimal corrector current to correct the harmonic, and σ_f is the width of the response. These fit parameters are used to determine the shape of each corrector currents and the optimal corrector currents for correction summarized in Tab. 2. There is a small difference in comparison of μ and σ between simulations and data with the largest difference of 0.27 A which is about 0.5% of the range of the power supplies.

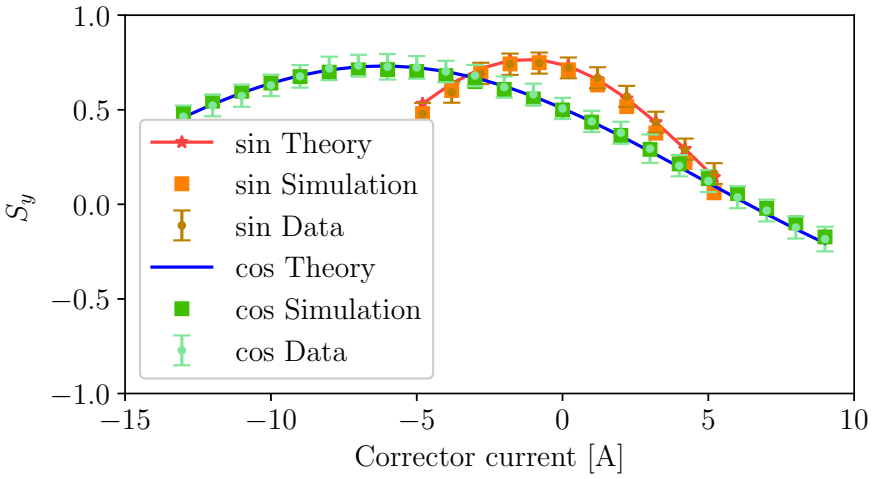

Figure 4: Harmonic scan of protons crossing $|G\gamma| = 3$ with a comparison between theory, simulations, and experimental data.

A scan using zgoubi at various initial currents of the sine and cosine corrector families shows the reliance on initial currents in the scan shown in Fig. 6.

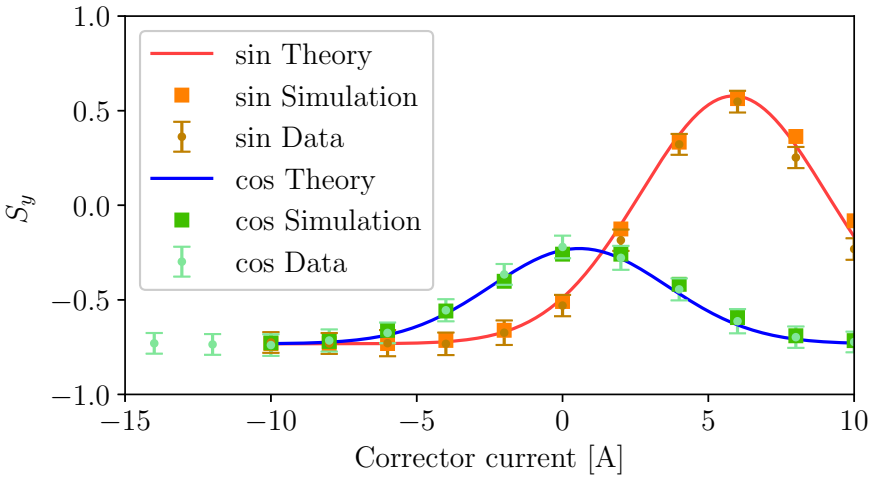

Figure 5: Harmonic scan of protons crossing $|G\gamma| = 4$ with a comparison between theory, simulations, and experimental data.

Table 2: Summary of fit data to proton harmonic scans.

k	source	$\mu_{\sin}$	$\sigma_{\sin}$	$A_{max,\sin}$	$\mu_{\cos}$	$\sigma_{\cos}$	$A_{max,\cos}$
3	scan data	-1.1821	3.8390	-0.7345	7.5322	-6.1607	-0.7468
3	simulation	-1.2997	3.5643	-0.7135	7.8536	-6.2140	-0.7124
4	scan data	5.8646	3.2160	0.5477	0.5740	3.2160	-0.2204
4	simulation	6.0330	3.2482	0.5638	0.7019	3.3593	-0.2585

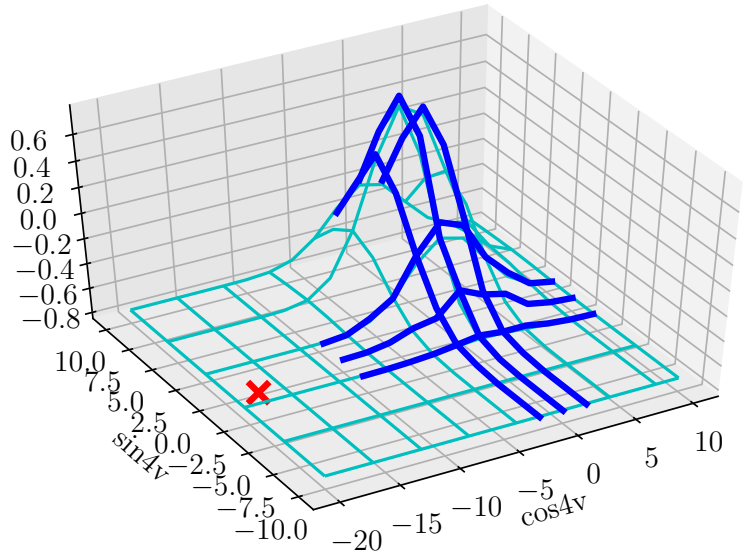

Figure 6: Harmonic scan of protons crossing the $|G\gamma| = 4$ resonance with initial currents at [-2,0,2] for the sine and cosine components. Dark blue lines are resulting simulation data. The light blue surface grid is reconstructed by fitting to the experimental data and extrapolating it to a larger range. The red 'X' marks corrector currents used in Run17, [sin4v,cos4v]=[0, -18].

3.2 Helion Harmonic Scans

With the experimental data of protons being well matched with simulation, the treatment is extended to helions. Fig. 7 shows a harmonic scan for helions crossing $|G\gamma| = 5$.

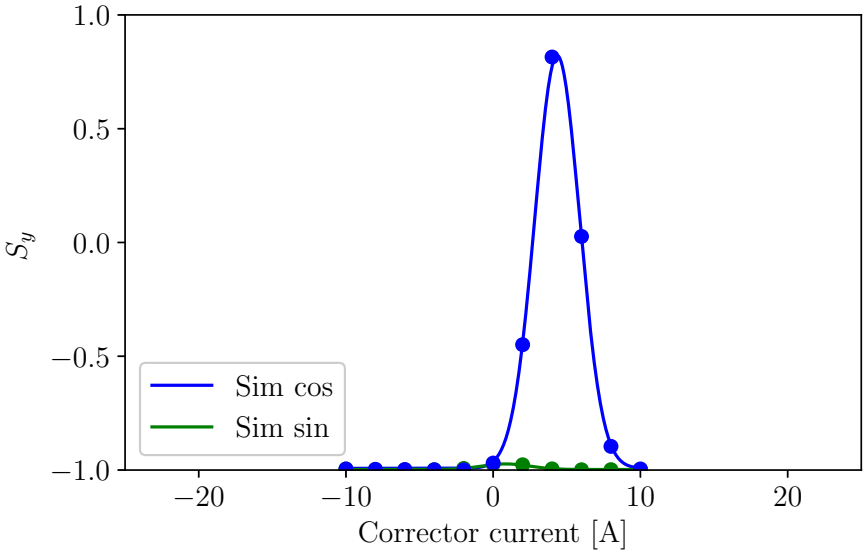

Figure 7: Helions crossing the $|G\gamma| = 5$ resonance. Correction of harmonic is insufficient and needs to be enhanced to spin-flip . To correct the orbit harmonic h=4, [sin4, cos4]=[2.797, 0.669] and to spin-flip: h=5 currents are [sin5, cos5]=[10.0, -18.0] and I_{max}=23.086.

Harmonic scans for the remaining imperfection resonances are shown in Sec. A.1 which show that there is sufficient corrector strength available. Fit results are summarized in Tab. 3 and corrector family currents and corresponding I_{max} in Tab. 4. Note more corrector current is available for the h=k resonances if the h=4, 5 harmonics are not corrected. The μ_f and σ_f are used to determine the optimal sinhv and coshv while remaining under the 25 A limit.

It is also worthwhile noting $|G\gamma| = 8$ and $|G\gamma|$=10 resonances have a strong dependence on the h=4 component of the orbit, evident by a comparison of Fig. 16 with Fig. 17 and of Fig. 20 with Fig. 21. Fig. 16 and Fig. 20 simulations use the orbit shown in Fig. 1 that uses sin4v=2.797 $B\rho(k)/B\rho(5)$ where Fig. 17 and Fig. 21 simulations use the orbit shown in Fig. 13 that uses sin4v=2.097 $B\rho(k)/B\rho(5)$. This variation can also be observed in the fit data of Tab. 3 and how benign the effect is on the other resonances.

With regard to ramping speed and helions, from Tab. 3 one can see the location of the correction, for the most part, does not change. The slower ramp rate results in a narrower distribution which means in the case of $G\gamma = 9$, correcting the h=9 orbit is likely not practical and this harmonic would need to be excited to induce a spin flip. These differences can be visualized with: Fig. 18 ($G\gamma = 9$ fast ramp) and Fig. 19 ($G\gamma = 9$ slow ramp); and Fig. 20 ($G\gamma = 10$ fast ramp) and Fig. 22 ($G\gamma = 10$ slow ramp);

Table 3: Summary of fit data for helion harmonic scans.

k	α	orbit	$\mu_{\sin}$	$\sigma_{\sin}$	$A_{max,\sin}$	$\mu_{\cos}$	$\sigma_{\cos}$	$A_{max,\cos}$
5	$\alpha_{helions,fast}$	Fig. 1	0.5200	1.5750	0.6843	4.2955	1.5288	0.8209
5	$\alpha_{helions,fast}$	Fig. 13	0.4746	1.2075	-0.9671	4.2225	1.4749	0.8159
6	$\alpha_{helions,fast}$	Fig. 1	1.2226	3.6268	0.8773	-0.2896	2.7384	0.8127
6	$\alpha_{helions,fast}$	Fig. 13	1.1615	3.6287	0.8823	-0.2372	2.7059	0.8205
7	$\alpha_{helions,fast}$	Fig. 1	3.1077	4.4358	0.8165	1.8801	4.5166	0.5680
7	$\alpha_{helions,fast}$	Fig. 13	2.9817	4.5565	0.8073	1.6875	4.5153	0.5617
8	$\alpha_{helions,fast}$	Fig. 1	-4.8460	4.8366	-0.6658	10.6646	5.5313	0.3322
8	$\alpha_{helions,fast}$	Fig. 13	1.9075	5.6127	0.8927	1.7186	5,3711	0.8653
9	$\alpha_{helions,fast}$	Fig. 1	-1.1232	5.2331	0.9987	-0.3165	3.9495	0.9779
9	$\alpha_{helions,fast}$	Fig. 13	-1.0890	5.0791	0.9993	-0.3154	3.9433	0.9814
9	$\alpha_{helions,slow}$	Fig. 13	-0.9737	4.7709	0.9550	-0.3320	2.989	0.6377
10	$\alpha_{helions,fast}$	Fig. 1	-23.6518	5.5783	0.9127	-0.4287	5.4708	0.5344
10	$\alpha_{helions,fast}$	Fig. 13	-3.5187	5.4745	0.8869	1.2351	5.4345	0.5923
10	$\alpha_{helions,slow}$	Fig. 13	-3.3476	3.0776	0.7155	0.7384	2.9718	-0.0992

Table 4: Current to correct the two major orbit harmonics (h=4, 5), current to correct or amplify the orbit harmonic corresponding to the resonance (h=k), and the resulting maximum current on any single dipole corrector (current in units of Amps).

Species	k	sin4v	cos4v	sin5v	cos5v	sinkv	coskv	I_{max}
Protons	3	-	-	-	-	0.897	-6.468	6.530
	4	-	-	-	-	0.0	18.0	24.306
Helions	5	2.797	0.669	-	-	10.0	-18.0	23.086
	6	4.393	1.051	0.817	6.748	-10.0	15.0	24.672
	7	5.733	1.371	1.067	8.806	-10.0	-10.0	24.246
	8	6.966	1.666	1.295	10.700	4.0	-13.0	24.491
	9	8.141	1.947	1.514	12.504	-1.074	0.0	17.924
	10	9.279	2.220	1.725	14.253	10.0	10.0	23.459

3.3 Resonance Crossing

Polarized helions crossing the $|G\gamma| = 5$ resonance with sufficient current to spin-flip is shown in Fig. 8. Simulations of particles crossing each resonance with no corrector current for the h=k harmonic is shown in Sec. A.2.2 and with corrector currents for optimized polarization transmission are shown in Sec. A.2.3.

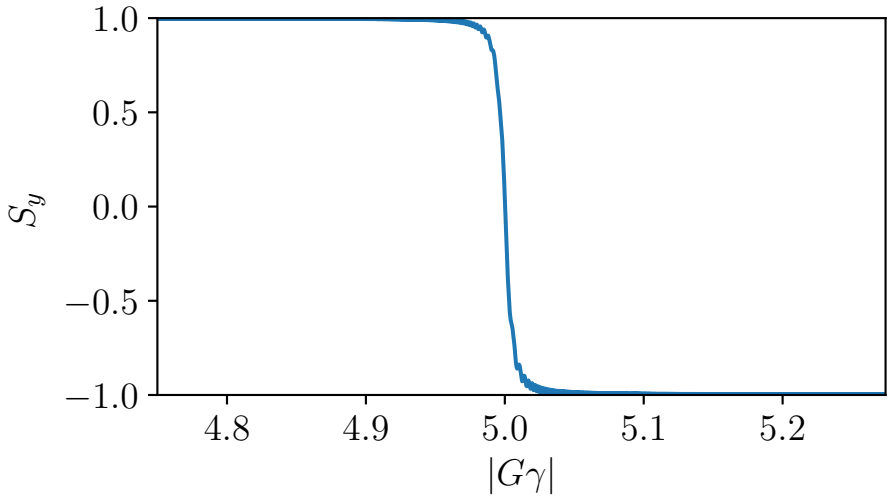

Figure 8: 1,000 helion particles crossing the $|G\gamma| = 5$ resonance with harmonic corrector strengths [sin4v, cos4v, sin5v, cos5v]=[2.797, 0.669, 10.0, -18.0] and $P_f = -99.18\%$.

3.3.1 Resonance crossing in close proximity to AC dipole cycle

Due to the proximity of the $|G\gamma|$ =8 and 10 imperfection resonances with the $|G\gamma| = 12 - \nu_y$ and $6 + \nu_y$ intrinsic resonances, simulations are performed to ensure that there is sufficient time for the AC dipole cycle and the spin-flip to occur in both of these nearby resonances. An AC dipole induces a spin flip through intrinsic spin resonances by driving large amplitude coherent oscillations so all particles sample the depolarizing vertical fields of quadrupoles. Intrinsic resonances occur when [3]

$$|G\gamma| = nP \pm \nu_y \tag{17}$$

where n is an integer and P is the superperiodicity, in Booster P=6. The two intrinsic resonances crossed by helions in the Booster occur at $|G\gamma| = 12 - \nu_y = 7.808$ and $|G\gamma| = 6 + \nu_y = 10.174$ [7–9]. The location of these resonances is adjusted with ν_y for a suitable resonance proximity parameter of $\delta_m = 0.01$ where

$$\delta_m = \nu_y - \nu_m - l \tag{18}$$

where l is the integer component of ν_y and ν_m is the AC dipole tune. The AC dipole tune is defined as,

$$\nu_m = \frac{f_m}{f_{rev}} \tag{19}$$

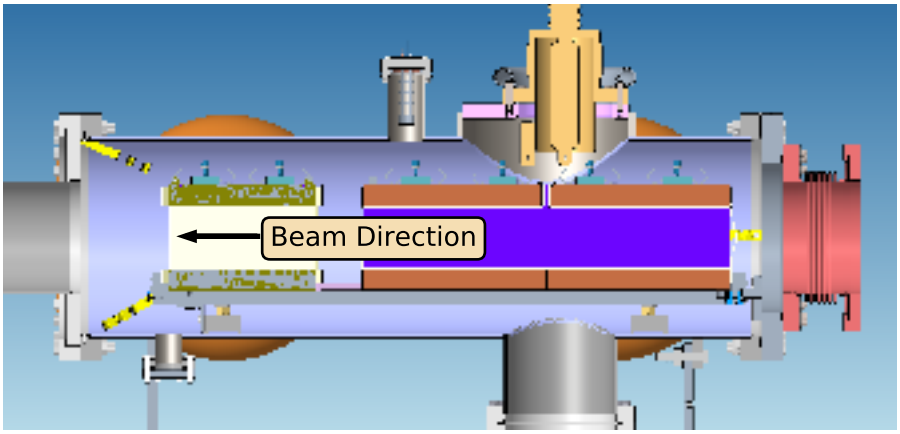

Figure 9: Cross section of the Booster AC dipole and tune meter upgrade.

where f_m=250 kHz is the frequency of the AC dipole and f_{rev} is the revolution frequency. The amplitude of these coherent oscillations is defined as

$$Y_{coh} = \frac{\beta_y}{4\pi} \frac{B_m l}{B\rho\delta_m} \tag{20}$$

where B_m is the AC dipole field and l is its length. The AC dipole installed in the E3 section is 50 cm long with a design maximum field of 5.0 mT [10]. The strength for $|G| = 12 - \nu_y$ is $B_m l = 2.38$ mT·m and $\delta_m = 0.007$, and for $|G\gamma| = 6 + \nu_y$ is $B_m l = 1.41$ mT·m with $\delta_m = 0.005$.

For the tracking results shown in Fig. 10 and Fig. 11 1,000 particles are tracked with $\varepsilon_{x,N\ 95\%} = \varepsilon_{y,N\ 95\%} = 3.5\ \mu m$ and $\sigma_p = 1.19 \times 10^{-3}$. As observed in this two sets of resonance crossing, the stable spin direction does not full spin-flip after crossing one and before crossing the other. Due to the proximity and strength of these nearby resonances, the stable spin direction is not fully aligned vertically. It is after crossing the pair of resonances that the stable spin direction returns to vertical and the spin-flip through each resonance can be observed with $P_f \sim 99\%$.

Results of 1,000 particles crossing the $|G\gamma| = 10$ and $|G\gamma| = 6 + \nu_y$ resonances with several machine configurations including: correction of h=10 orbit components so $|G\gamma| = 10$ does not spin-flip and $B_m l$ =3.5 mT $\cdot$ m for the 100% spin-flip through the $|G\gamma| = 6 + \nu_y$ resonance; sin10v, cos10v= 20 A, 11 A to spin-flip through the $|G\gamma| = 10$

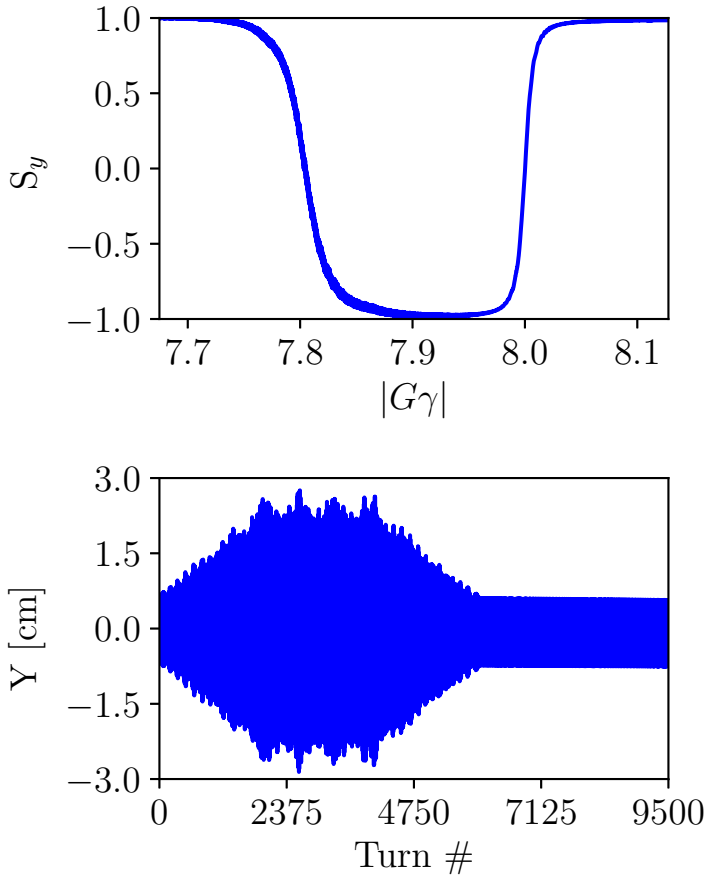

Figure 10: Helions crossing the $|G\gamma| = 12 - \nu_y$ resonance followed by the $|G\gamma| = 8$ resonance with harmonic corrector strenghts [sin4v, cos4v, sin5v, cos5v, sin8v, cos8v]=[6.966, 1.666, 1.295, 10.700, 4.0, -13.0]. The AC dipole ramp is 2000 turns up, 2000 turns flat, and 2000 turns down. AC dipole parameters used are $B_m l = 2.38$ mT·m and $\delta_m = 0.007$ with $P_f = 99.06$.

resonance and $B_m l$ =3.5 mT $\cdot$ m for the 100% spin-flip through the $|G\gamma| = 6 + \nu_y$ resonance; sin10v, cos10v= 20 A, 11 A to spin-flip to spin-flip through $|G|a = 10$ and $B_m l$ =0.0 mT $\cdot$ m for to observe polarization loss through the $|G\gamma| = 6 + \nu_y$ resonance; partial h=10 correction with sin10v, cos10v= 0 A, 5 A to observe polarization loss through $|G\gamma| = 10$ and $B_m l$ =3.5 mT $\cdot$ m for to spin-flip through the $|G\gamma| = 6 + \nu_y$ resonance. Note in the case that $B_m l$ =3.5 mT $\cdot$ m that the vertical component of the polarization vector returns to vertical between the $|G\gamma| = 10$ and $|G\gamma| = 6 + \nu_y$ resonances. In the case where the $|G\gamma| = 10$ and $|G\gamma| = 6 + \nu_y$ resonances are enhanced to induce a spin-flip, the vertical component of the stable spin direction does not return to vertical between the two. The polarization after both the resonances are crossed is where the efficiency of each spin-flip is account.

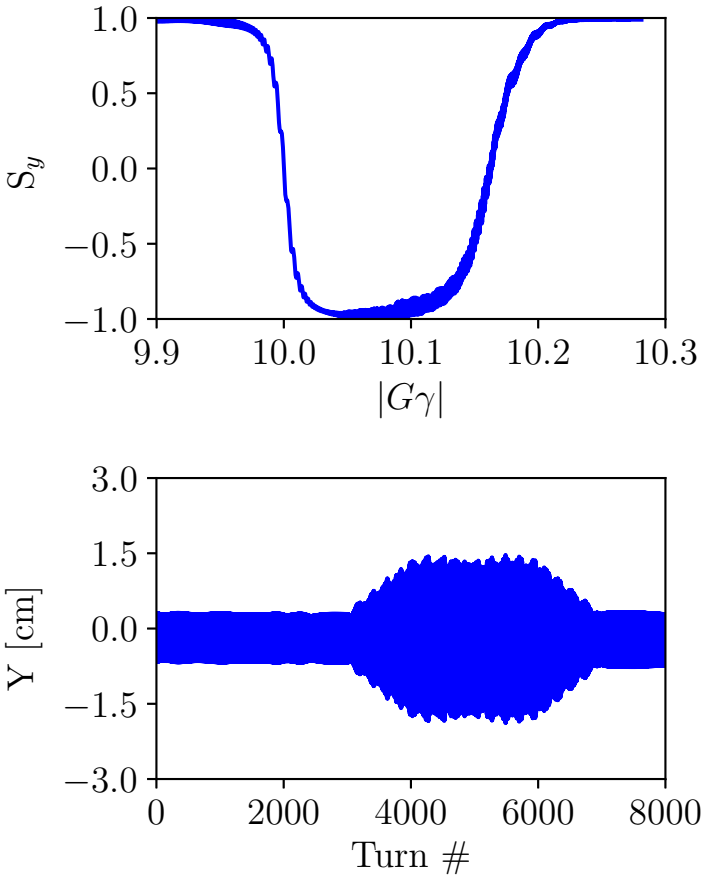

Figure 11: 1,000 helion particles crossing the $|G\gamma| = 6 + \nu_y$ resonance followed by the $|G\gamma| = 10$ resonance with harmonic corrector strengths [sin4v, cos4v, sin5v, cos5v, sin8v, cos8v]=[9.279, 2.220, 1.725, 14.253, 10.0, 10.0]. The AC dipole ramp is 2000 turns up, 2000 turns flat, and 2000 turns down. AC dipole parameters used are $B_m l = 1.41$ mT·m and $\delta_m = 0.005$ with $P_f = 99.08$.

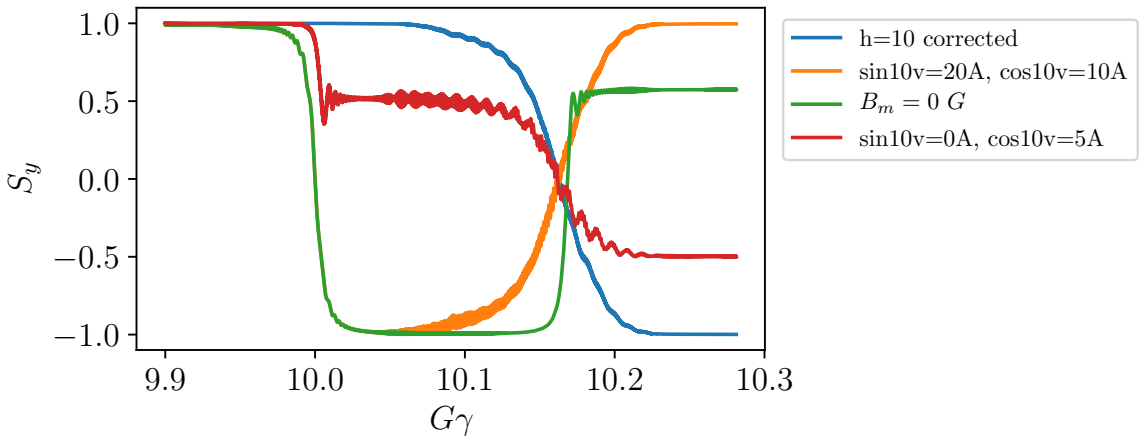

Figure 12: Results of 1,000 helion particles crossing the $|G\gamma| = 10$ and $|G\gamma| = 6 + \nu_y$ resonances for several machine configurations.

4 Conclusion

Through implementation of alignment errors into the zgoubi model of the booster, harmonic scan data of protons crossing $|G\gamma| = 3,\ 4$ was successfully replicated. This methodology was extended to the case of polarized helions where it was determined that there is sufficient corrector current available to preserve polarization through the $|G\gamma| = 5,\ 6,\ 7,\ 8,\ 9,\ 10$ resonances. In the case of $|G\gamma| = 8$ and $|G\gamma| = 10$ which are crossed in close proximity of the AC dipole cycles show there is still lossless transmission of polarization.

5 Acknowledgements

A special thanks to Nick Kling and Petra Adams that took the data set used.

A Helions Data

A.1 Helion Harmonic Scans

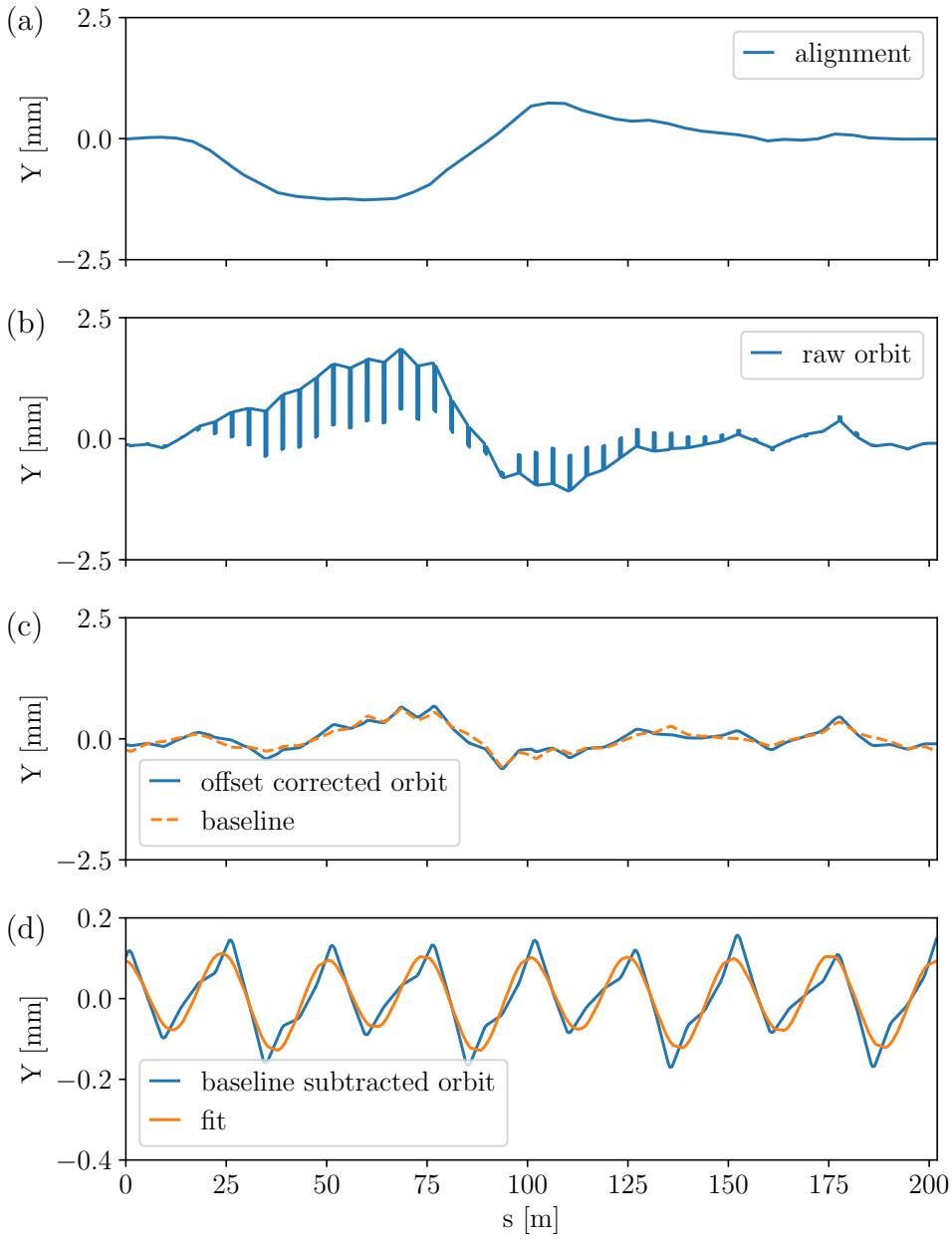

Figure 13: a) Vertical quadrupole misalignments in the Booster scaled to 65% to match h=4 data; b) orbit output from zgoubi where discontinuities result from the use of CHANGREF through quadrupoles; c) Orbit after incorporating misalignments; d) Baseline subtracted orbit for helions crossing the $|G\gamma| = 8$ resonance after the h=4, 5 harmonics have been corrected with the addition of h=8. This example has a corrector currents [sin4v, cos4v, sin5v, cos5v, sin8v, cos8v]=[2.797 $B\rho/B\rho(5)$, 0.669 $B\rho/B\rho(5)$, 0.520 $B\rho/B\rho(5)$, 4.296 $B\rho/B\rho(5)$, 4.0 ,-13.0]. The components of the fit results are: [sin4, cos4, sin5, cos5, sin8, cos8]=[0.000254, -0.000022, -0.000019, -0.000043, -0.000216, 0.000997].

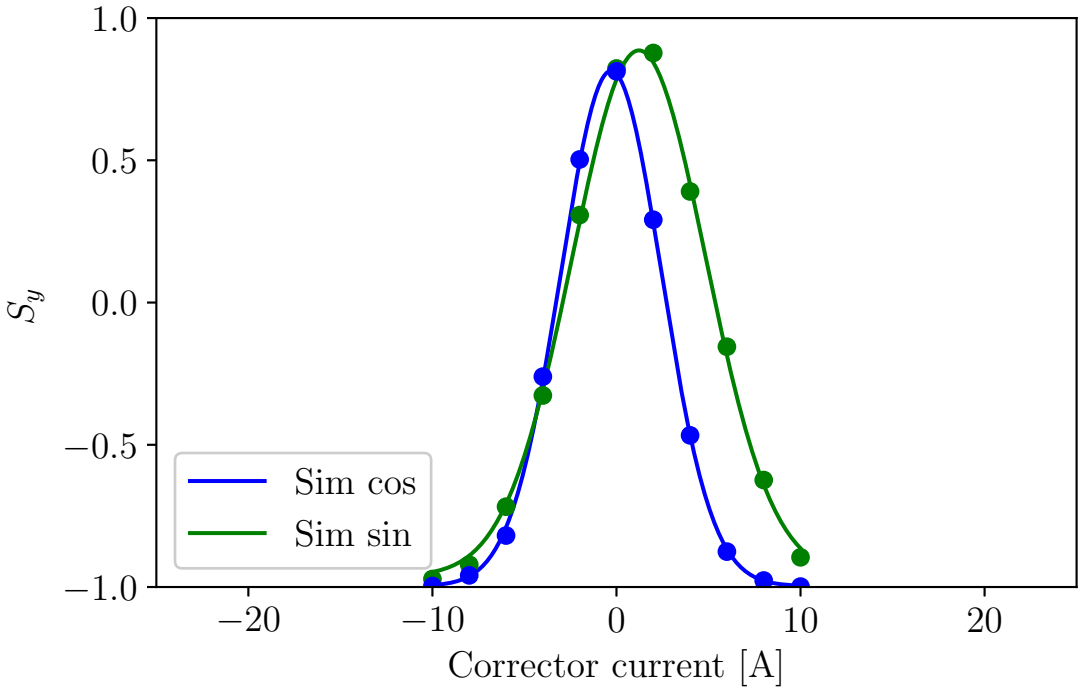

Figure 14: Helion harmonic scan of current for h=6 after correcting for the h=4, 5 harmonics. Can achieve a full spin-flip with sin8v=6.2 A and cos8v=-10 A which results in I_{max}=18.44 A. Fit data found in Tab. 3.

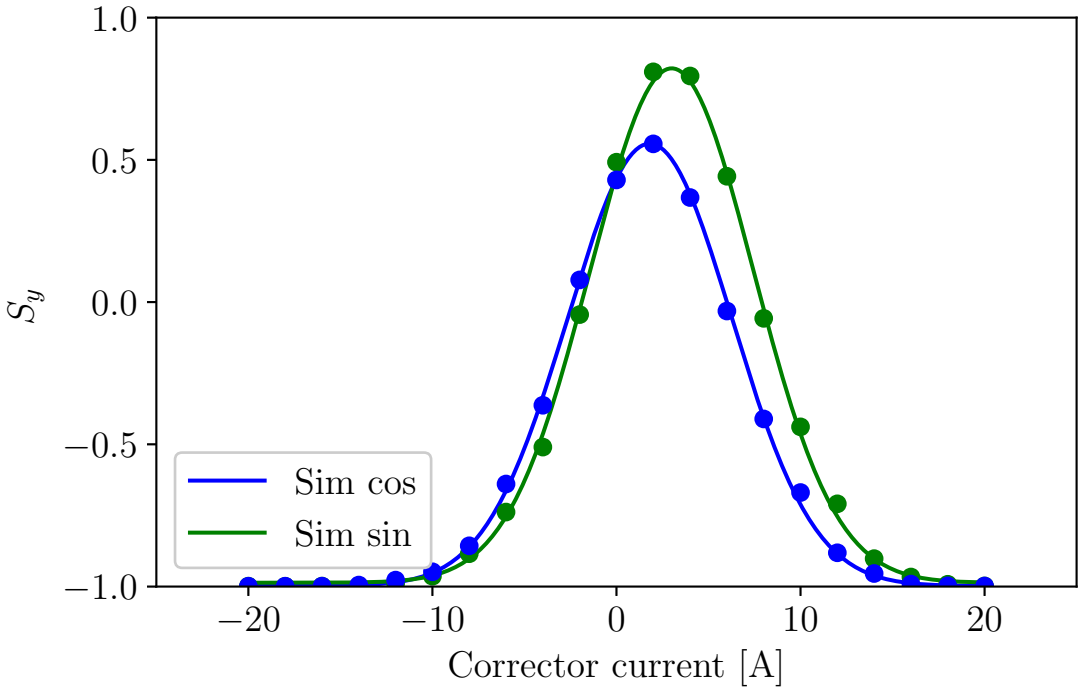

Figure 15: Helion harmonic scan of current for h=7 after correcting for the h=4, 5 harmonics. Can achieve a full spin-flip with sin7v=-10 A and cos7v=-10 A which results in I_{max}=24.14 A. Fit data found in Tab. 3.

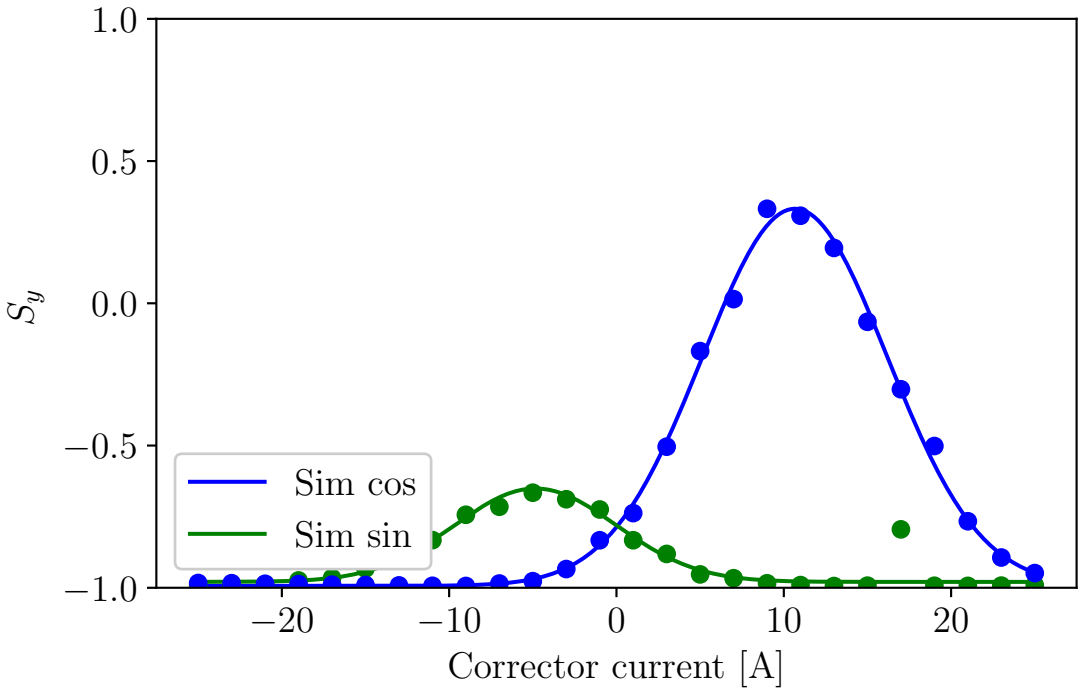

Figure 16: Helion harmonic scan of current for h=8 after correcting for the h=4, 5 harmonics. Can achieve a full spin-flip with sin8v=2.9 A and cos8v=-18 A which results in I_{max}=24.92 A. Fit data found in Tab. 3.

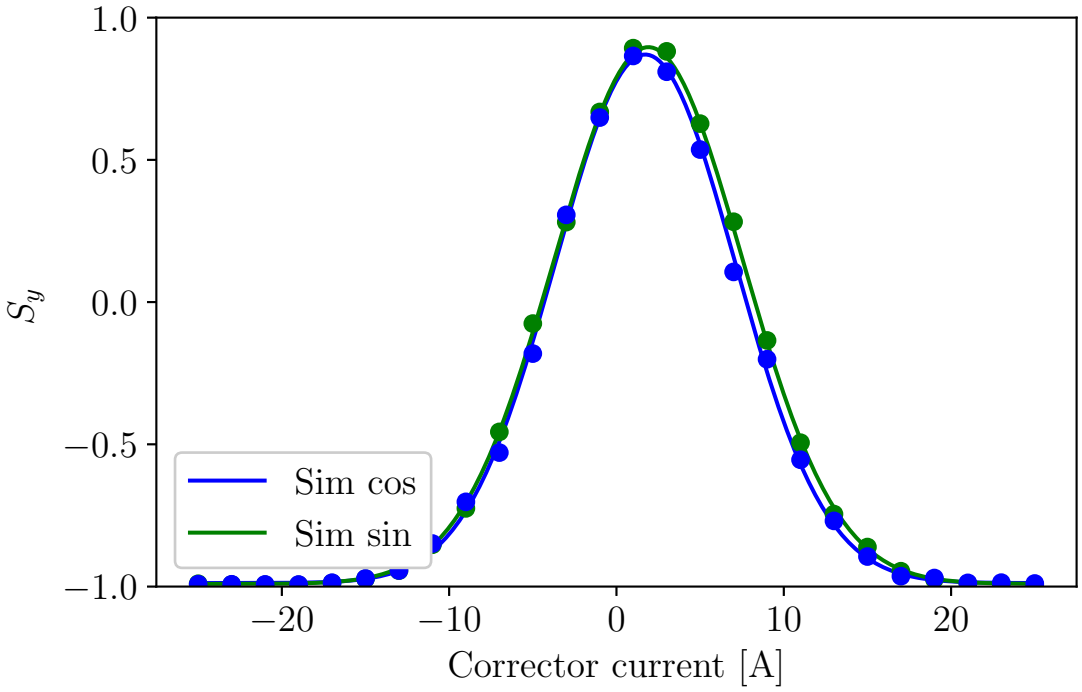

Figure 17: Helion harmonic scan of current for h=8 after correcting for the h=4, 5 harmonics. Can achieve a full spin-flip with sin8v=2.9 A and cos8v=-18 A which results in I_{max}=24.92 A. Fit data found in Tab. 3.

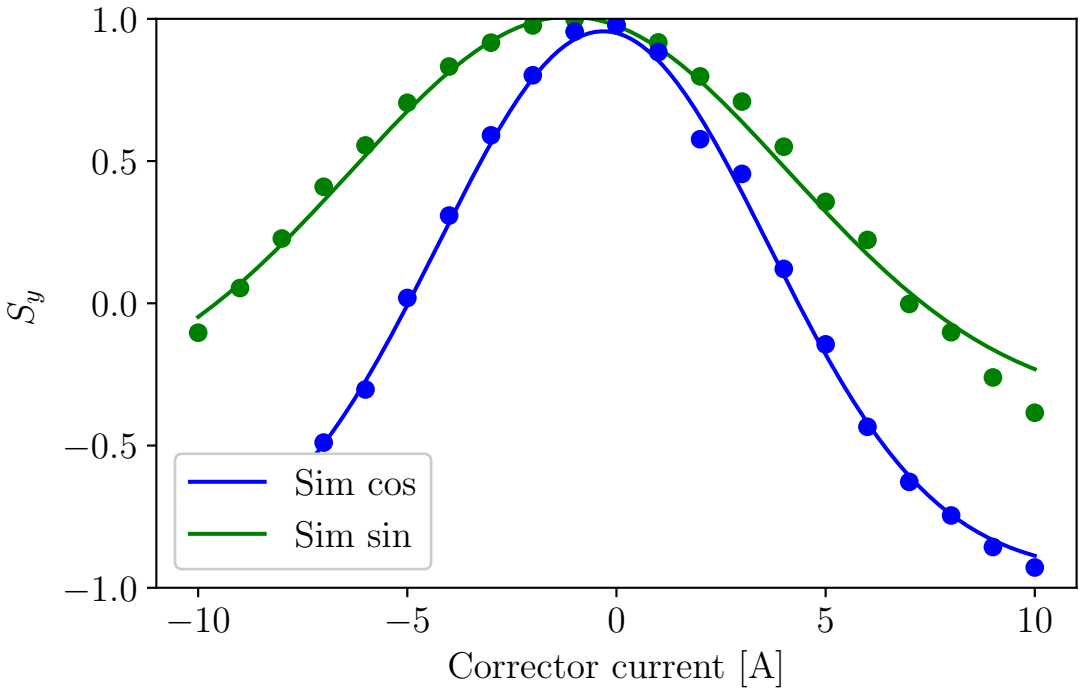

Figure 18: Helion harmonic scan of current for h=9 after correcting for the h=4, 5 harmonics. Can achieve a full spin-flip with sin9v= A and cos9v= A which results in I_{max}= A. Fit data found in Tab. 3.

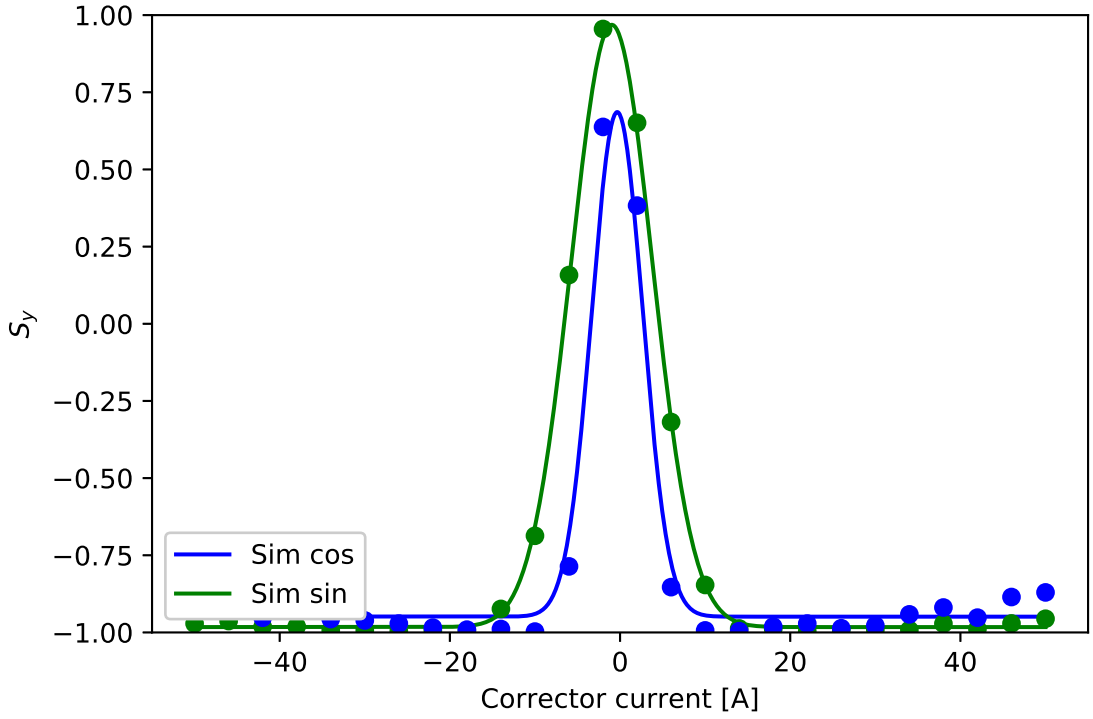

Figure 19: Slow ramp helion harmonic scan of current for h=9 after correcting for the h=4, 5 harmonics. Can achieve a full spin-flip with sin9v= A and cos9v= A which results in I_{max}= A. Fit data found in Tab. 3.

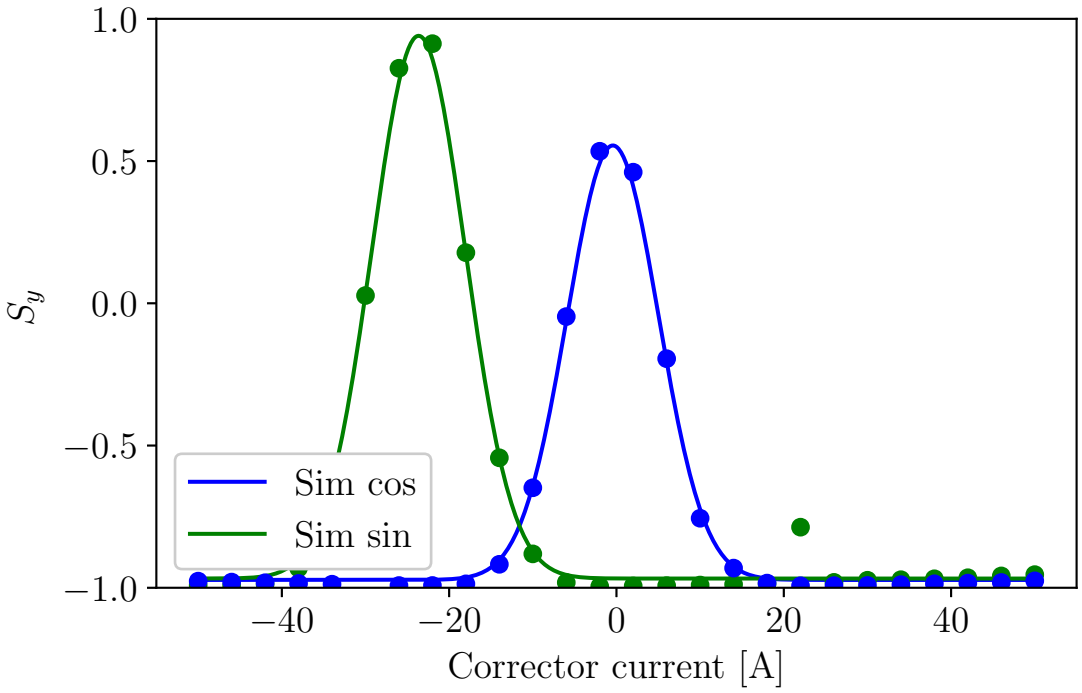

Figure 20: Helion harmonic scan of current for h=10 after correcting for the h=4, 5 harmonics. Can achieve a full spin-flip with sin10v=9 A and cos10v=10 A which results in I_{max}= 24.94A. Fit data found in Tab. 3.

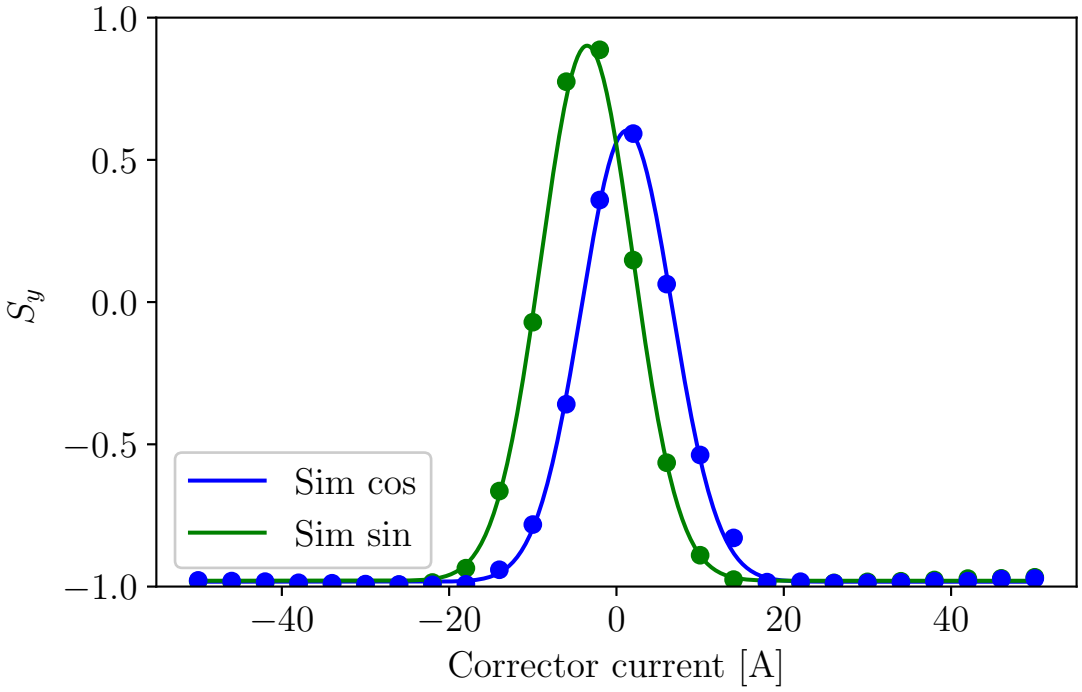

Figure 21: Helion harmonic scan of current for h=10 after correcting for the h=4, 5 harmonics. Can achieve a full spin-flip with sin10v=9 A and cos10v=10 A which results in I_{max}= 24.94A. Fit data found in Tab. 3.

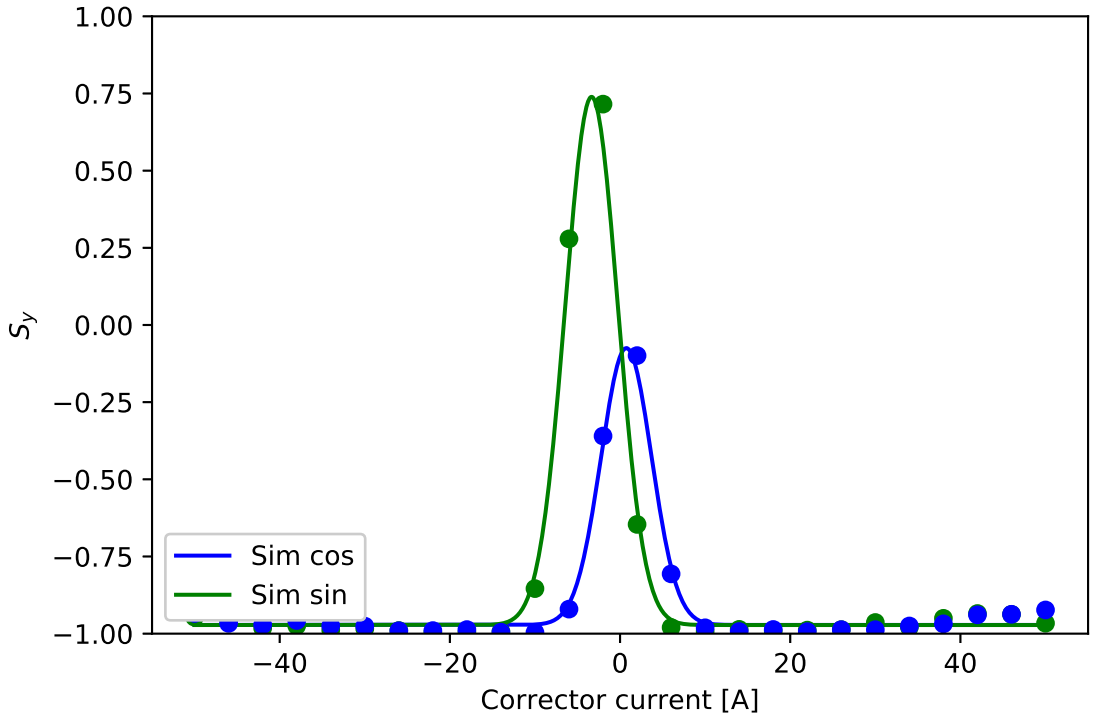

Figure 22: Slow ramp helion harmonic scan of current for h=10 after correcting for the h=4, 5 harmonics. Can achieve a full spin-flip with sin10v=9 A and cos10v=10 A which results in I_{max}= 24.94A. Fit data found in Tab. 3.

A.2 Resonance Crossing

A.2.1 Static

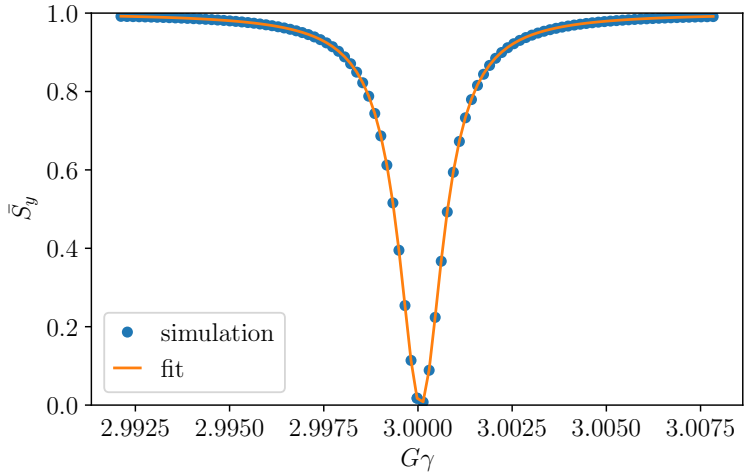

Figure 23: Static depolarization of protons at $|G\gamma| = 3$, ϵ_k=0.000714.

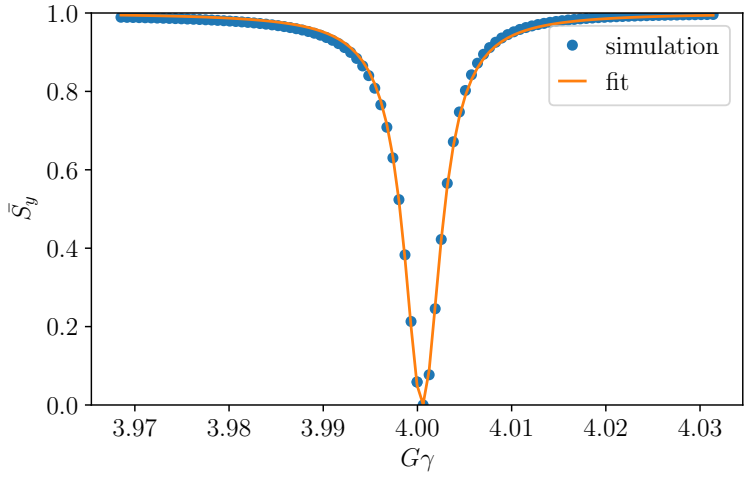

Figure 24: Static depolarization of protons at $|G\gamma| = 4$, ϵ_k=0.002396.

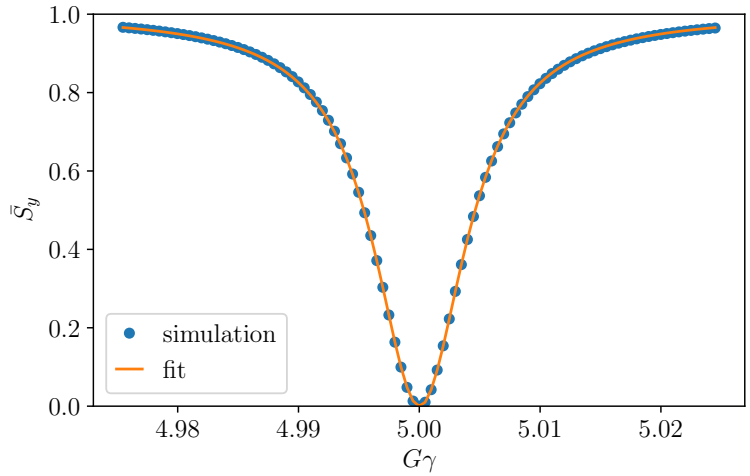

Figure 25: Static depolarization of helions at $|G\gamma| = 5$, ϵ_k=0.004492.

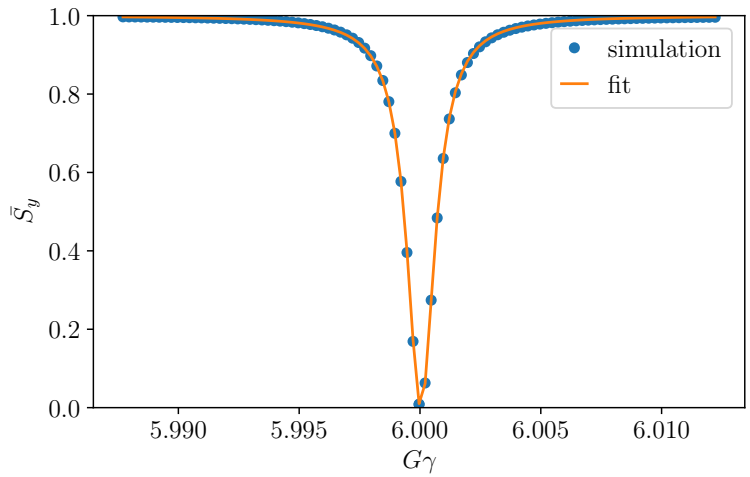

Figure 26: Static depolarization of helions at $|G\gamma| = 6$, ϵ_k=0.000716.

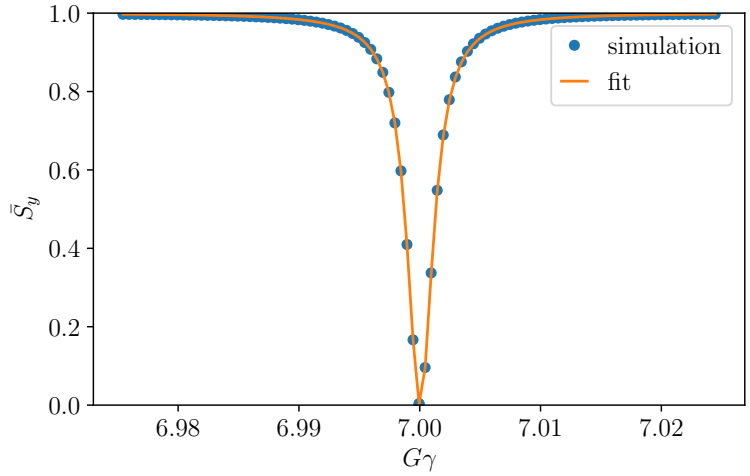

Figure 27: Static depolarization of helions at $|G\gamma| = 7$, ϵ_k=0.001158.

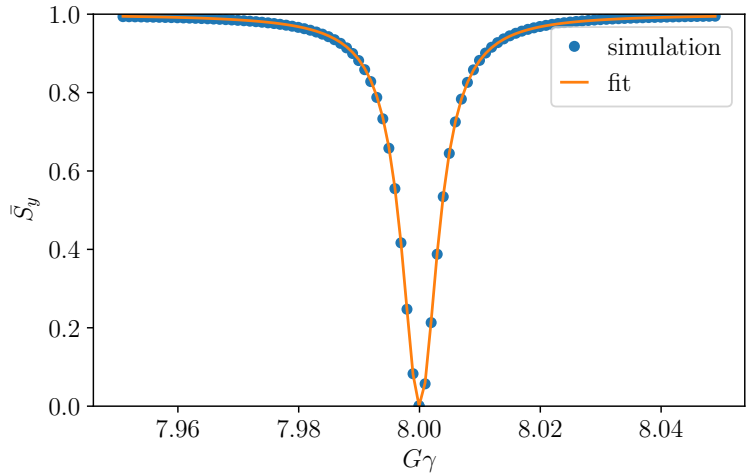

Figure 28: Static depolarization of helions at $|G\gamma| = 8$, ϵ_k=0.003834.

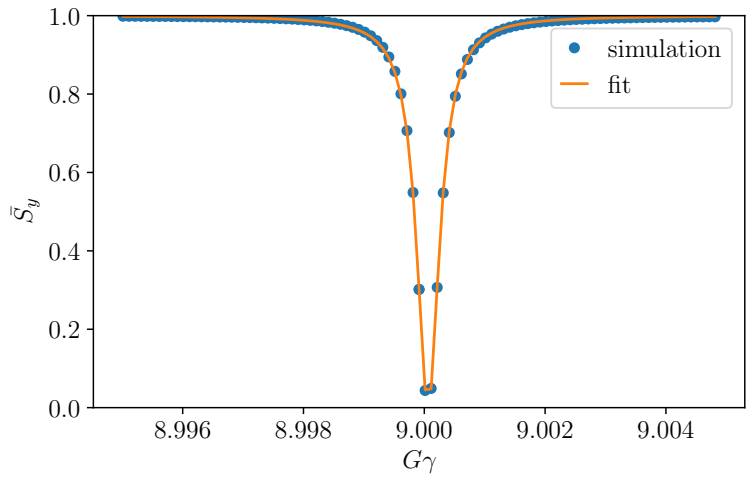

Figure 29: Static depolarization of helions at $|G\gamma| = 9$, ϵ_k=0.000239.

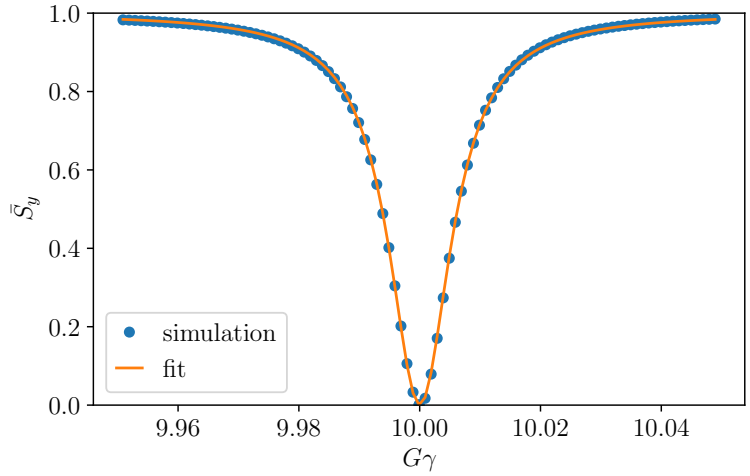

Figure 30: Static depolarization of helions at $|G\gamma| = 10$, ϵ_k=0.006252.

A.2.2 Froissart-Stora

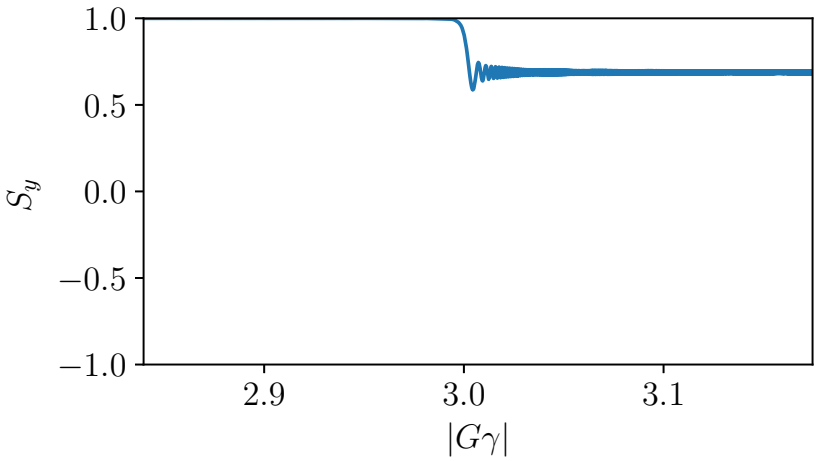

Figure 31: Protons crossing the $|G\gamma| = 3$ resonance, $P_f = 69.55$.

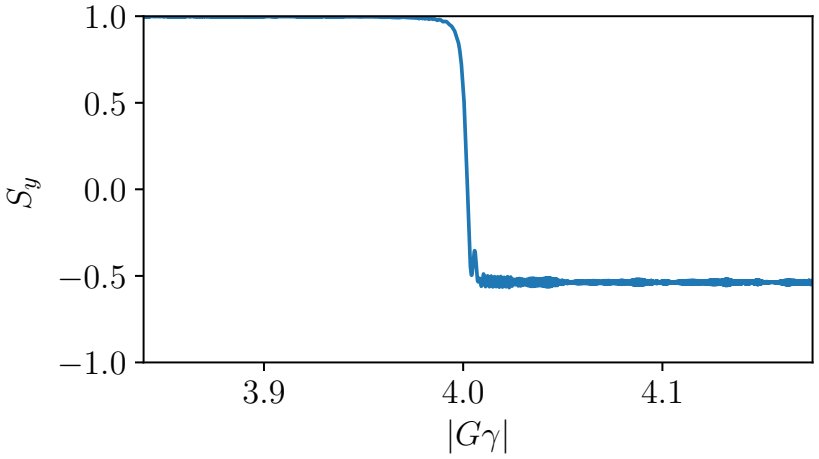

Figure 32: Protons crossing the $|G\gamma| = 4$ resonance, $P_f = -53.50$.

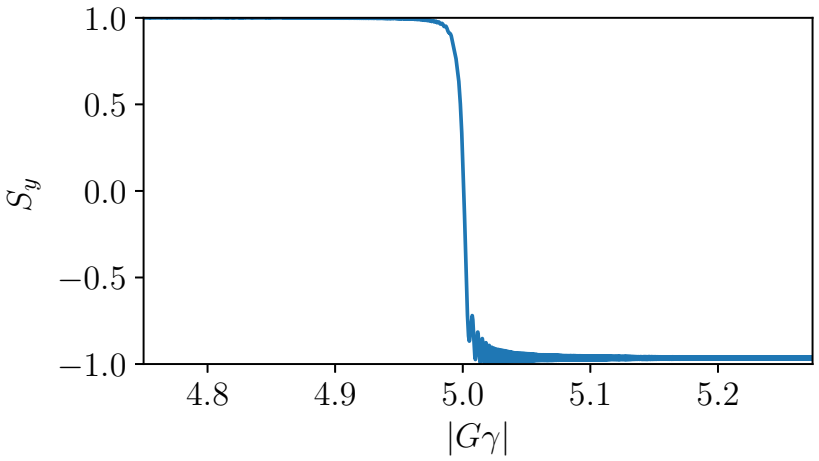

Figure 33: Helions crossing the $|G\gamma| = 5$ resonance, $P_f = -96.86$.

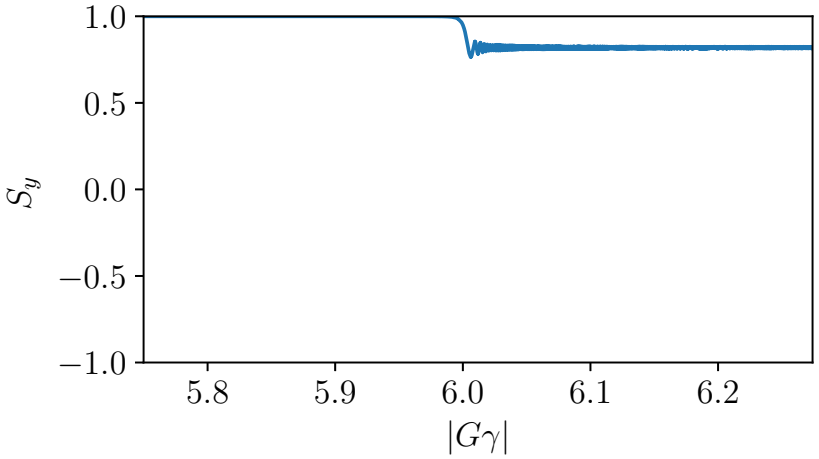

Figure 34: Helions crossing the $|G\gamma| = 6$ resonance, $P_f = 81.49$.

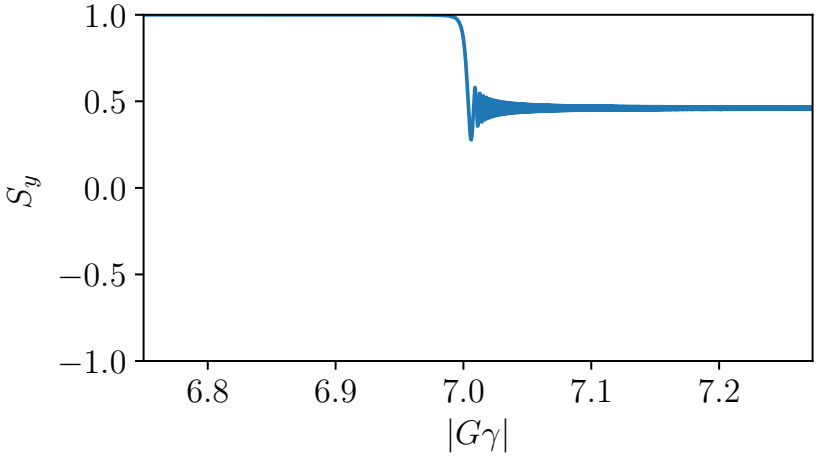

Figure 35: Helions crossing the $|G\gamma| = 7$ resonance, $P_f = 45.94$.

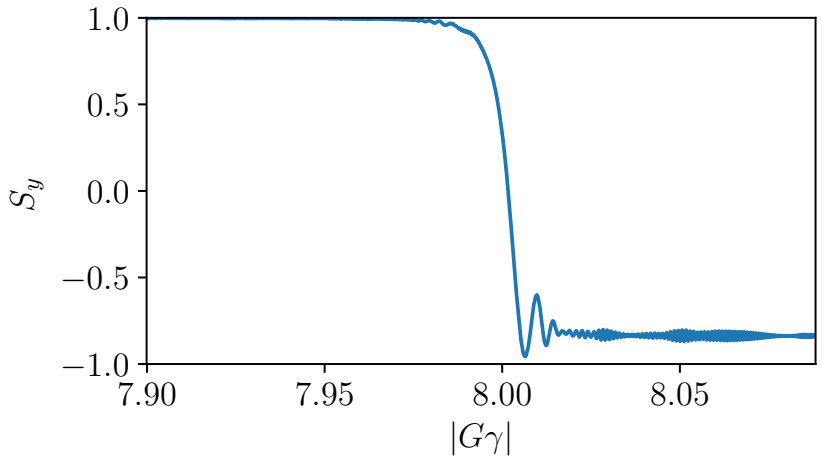

Figure 36: Helions crossing the $|G\gamma| = 8$ resonance, $P_f = -83.36$.

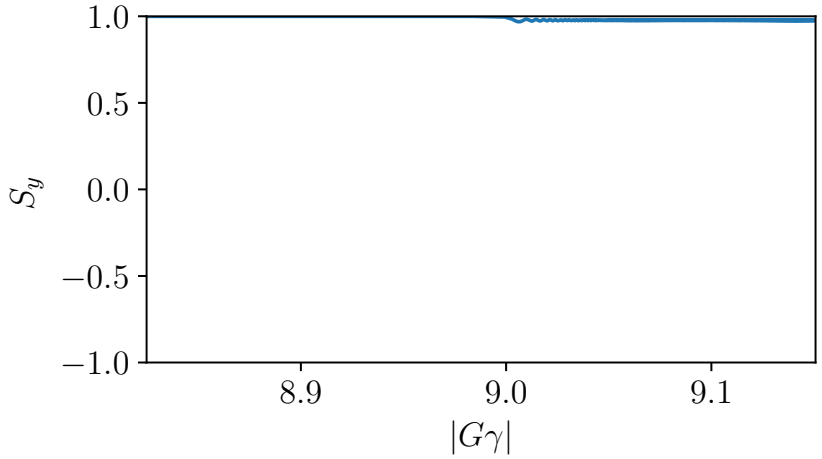

Figure 37: Helions crossing the $|G\gamma| = 9$ resonance, $P_f = 97.91$.

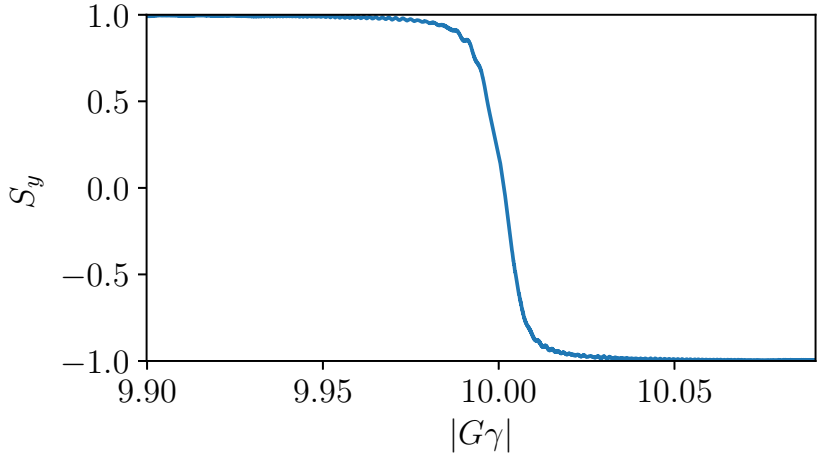

Figure 38: Helions crossing the $|G\gamma| = 10$ resonance, $P_f = -99.42$.

A.2.3 With Harmonics

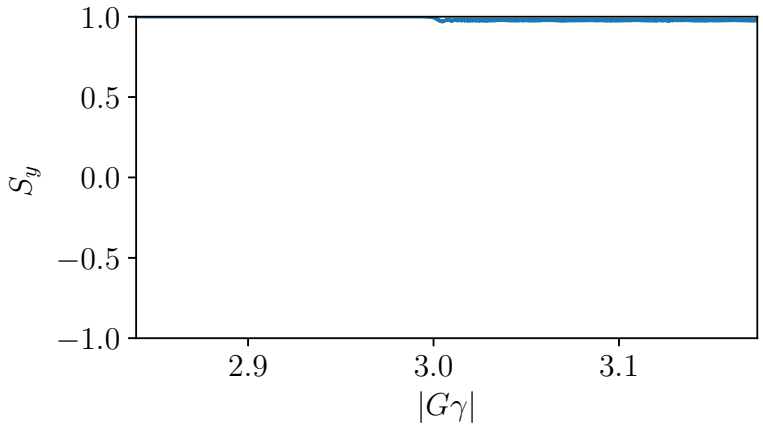

Figure 39: Protons crossing the $|G\gamma| = 3$ resonance. Harmonic corrector family strengths found in Tab. 4.

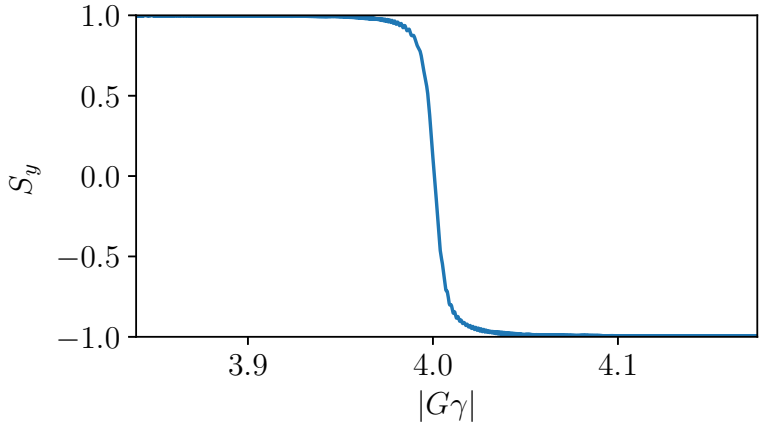

Figure 40: Protons crossing the $|G\gamma| = 4$ resonance. Harmonic corrector family strengths found in Tab. 4.

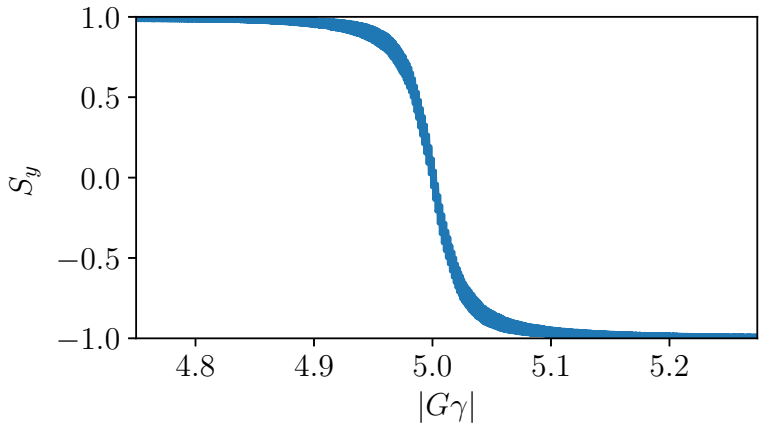

Figure 41: Helions crossing the $|G\gamma| = 5$ resonance. Harmonic corrector family strengths found in Tab. 4.

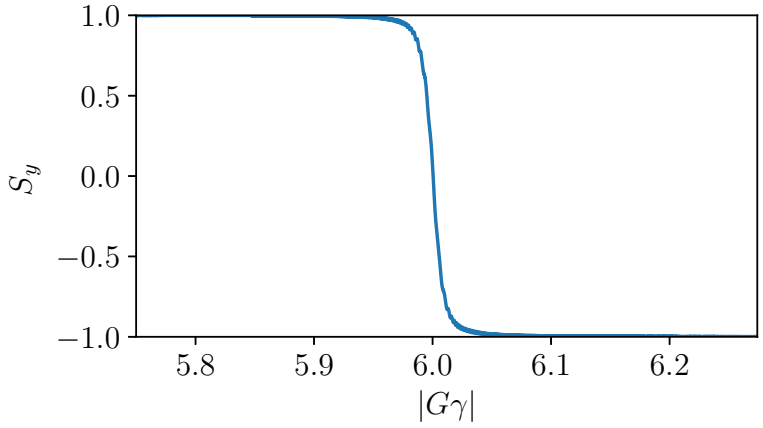

Figure 42: Helions crossing the $|G\gamma| = 6$ resonance. Harmonic corrector family strengths found in Tab. 4.

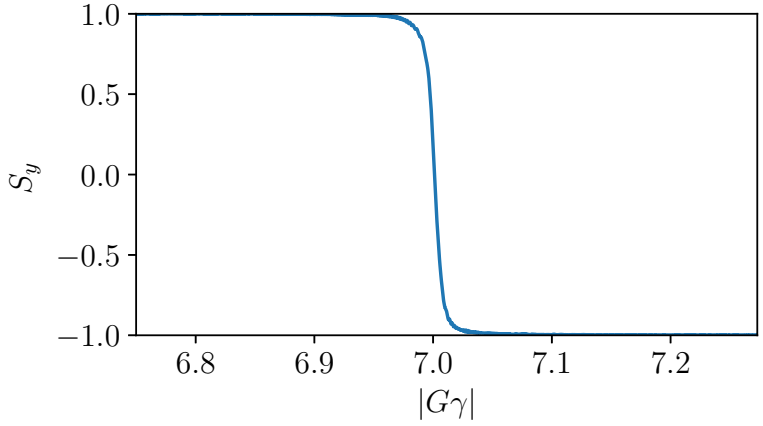

Figure 43: Helions crossing the $|G\gamma| = 7$ resonance. Harmonic corrector family strengths found in Tab. 4.

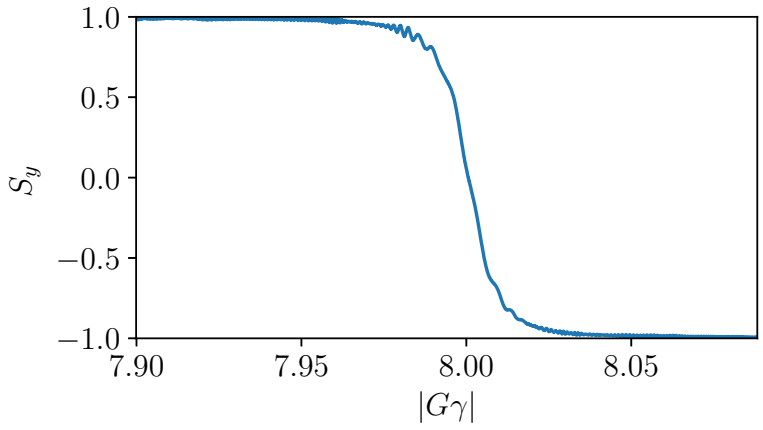

Figure 44: Helions crossing the $|G\gamma| = 8$ resonance. Harmonic corrector family strengths found in Tab. 4.

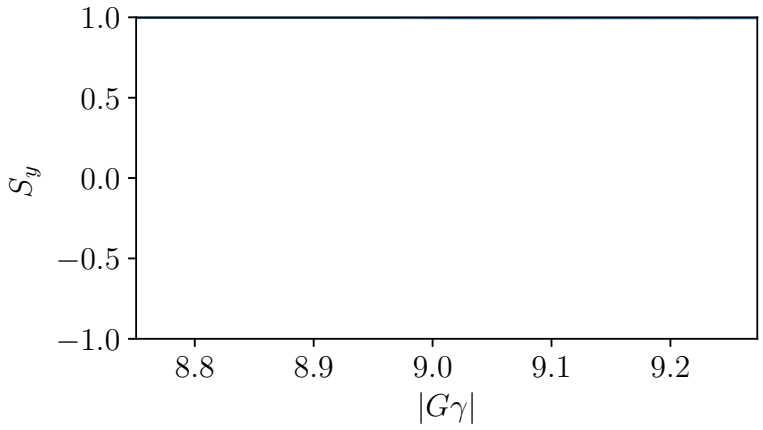

Figure 45: Helions crossing the $|G\gamma| = 9$ resonance. Harmonic corrector family strengths found in Tab. 4.

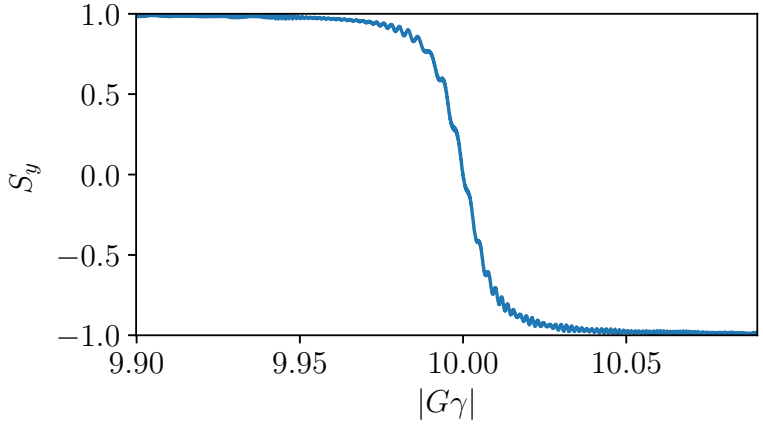

Figure 46: Helions crossing the $|G\gamma| = 10$ resonance. Harmonic corrector family strengths found in Tab. 4.

References

[1] J. Maxwell, C. Epstein, R. Milner, J. Alessi, E. Beebe, A. Pikin, J. Ritter, and A. Zelenski, International Journal of Modern Physics: Conference Series **40**, 1660102 (2016), https://doi.org/10.1142/S2010194516601022 .

[2] E. Aschenauer et al., in *Proceedings of RIKEN BNL Research Center Workshop* (2011).

[3] S. Y. Lee, *Spin Dynamics and Snakes in Synchrotrons* (World Scientific Publishing Company Incorporated, 1997).

[4] S. Y. Lee, *Accelerator Physics* (World Scientific Publishing Company Incorporated, 2012).

[5] R. Thern, *Booster Ring Correction Magnets*, Booster Tech Note 224 (1994).

[6] C. Yu et al., "AGS Booster Adjustment Report," (2015), unpublished.

[7] K. Hock et al., *Intrinsic Resonances and AC-Dipole simulations of* ^{3}*He in the AGS-Booster*, C-AD Tech Note 597 (2017).

[8] K. Hock et al., *Overcoming proton and* ^{3}*He Intrinsic Resonances in the AGS Booster with an ac dipole*, C-AD Tech Note 601, www.osti.gov/servlets/purl/1469789 (2018).

[9] K. Hock et al., in *Proceedings IPAC 2018 Conference.* Vancouver, Canada (accelconf.web.cern.ch/AccelConf/ipac2018/papers/tupaf005.pdf, 2018).

[10] N. Tsoupas et al., in *Proceedings CAARI 2018 Conference.* Dallas, USA (2018).